


Please cite the Published Version

Beake, BD, Liskiewicz, TW , Bird, A and Shi, X (2020) Micro-scale impact testing - a new approach to studying fatigue resistance in hard carbon coatings. Tribology International, 149. p. 105732. ISSN 0301-679X

DOI: <https://doi.org/10.1016/j.triboint.2019.04.016>

Publisher: Elsevier

Version: Accepted Version

Downloaded from: <https://e-space.mmu.ac.uk/623039/>

Usage rights:  [Creative Commons: Attribution-Noncommercial-No Derivative Works 4.0](#)

Additional Information: This is an Author Accepted Manuscript in Tribology International published by Elsevier.

Enquiries:

If you have questions about this document, contact openresearch@mmu.ac.uk. Please include the URL of the record in e-space. If you believe that your, or a third party's rights have been compromised through this document please see our Take Down policy (available from <https://www.mmu.ac.uk/library/using-the-library/policies-and-guidelines>)

**Micro-scale Impact testing - a new approach to studying fatigue resistance in hard
carbon coatings**

Ben D. Beake^{1,*}, Tomasz W. Liskiewicz², Andrew Bird¹ and Xiangru Shi^{2,3}

1 Micro Materials Ltd, Willow House, Yale Business Village, Ellice Way, Wrexham, LL13
7YL, United Kingdom

2 Institute of Functional Surface, School of Mechanical Engineering, University of Leeds,
Woodhouse Lane, Leeds LS2 9JT, United Kingdom

3 School of Materials Science and Engineering, Jiangsu Key Laboratory for Advanced
Metallic Materials, Southeast University, Nanjing 211189, China

*Corresponding author: Tel: +44 1978 261615; e-mail: ben@micromaterials.co.uk

Keywords:- impact; fatigue; DLC; micro-scale; micro-tribology

Abstract

Improving the fatigue resistance of DLC coatings under highly loaded repetitive contact is an important step to increasing their performance in demanding applications. The nano-impact test has been shown to be effective at highlighting differences in resistance to contact damage in thin hard carbon coatings deposited on hardened steel. A novel micro-scale rapid impact test capability capable of producing repetitive impacts at significantly higher strain rate and energy than in the nano-impact test has been developed recently enabling the study of coating fatigue with less sharp spherical indenters than in the nano-impact test.

Results with the new micro-impact technique on two commercial hard carbon coatings (Graphit-iC and Dymon-iC from Teer Coatings) on tool steel are presented. The role of coating mechanical properties on the fatigue resistance and the load-sensitivity of the impact failure mechanism is discussed. The harder coating with higher sp^3/sp^2 bonded C (Dymon-iC) was found to be significantly less durable under fatigue loading than the softer Graphit-iC. Reasons for the observed differences are discussed.

1. Introduction

Amorphous carbon films (commonly known as Diamond-like carbon or DLC) combine high hardness and wear resistance with low friction and are increasingly used as protective coatings in wide ranging industrial applications in automotive engines, as coated tools, and also in biomedical and MEMS devices, as antireflective coatings and in corrosion protection [1-4]. Their mechanical properties can be tuned to meet different requirements by changing the hybridisation of carbon atoms and the hydrogen content in the films [1]. The carbon-carbon bonding in amorphous carbon films is predominantly a mixture of C-C sp^3 (diamond) and C-C

sp^2 (graphite) [5]. To an extent hardness and wear properties are controlled by the sp^3/sp^2 ratio. Adding hydrogen increases sp^3 bonding and makes the coatings more diamond-like.

The performance of DLC coatings in many of these applications is limited by their resistance to contact damage [6,7] and typically they behave poorly at higher load despite being hard and elastic. Jiang and Arnell have shown that in pin-on-disk tests DLC films that exhibited very low rates of wear under low contact pressure sliding were susceptible to abrupt increases in wear rate as the pressure increases beyond a critical threshold at higher load [8]. The problem is exacerbated with hard DLC films are deposited on more ductile (soft/compliant) substrates which provide inadequate load support at higher load. Cracking of DLC films on various relatively soft and lower modulus substrates (TiAl64V [6-7], stainless steel [9], glass [10,11], aluminium [12]) on spherical indentation by small (5 or 10 μm) end radius diamond probes has been extensively studied with focussed ion beam (FIB) employed to determine sub-surface cracking. In these cases pop-ins during loading are commonly seen. Plastic deformation of the substrate is followed by circumferential cracks at the edge of the indent and radial cracks underneath the indent, which can ultimately result in cohesive and adhesive failures [6,9].

Common strategies to improve the resistance to contact damage include deposition of adhesion promoting interlayers, multilayering, changing sp^3/sp^2 through bias control, gradient layers, metal doping, deposition of load-supporting sub-layers [13-25]. Bernoulli and co-workers have reported that for biomedical applications deposition of a ductile α -Ta interlayer with elastic properties close to that of the DLC film was able to reduce the severity of ring cracking when indented by a 10 μm probe to 500 mN, which finite element analysis (FEA) suggested was due to the stress being distributed across the coating-interlayer and interlayer-substrate interfaces [6]. Hard DLC films commonly have high compressive internal stresses. Metal doping can effectively lower these stresses. To improve the bonding between the covalent bonded carbon

film to the metallic substrate interlayers which are chemically compatible with both the film and substrate (e.g. W, Cr) have been demonstrated to improve adhesion. A further refinement is a graded interlayer design from metallic to carbide to pure carbon which can reduce stresses in the a-C layer and improve adhesion [3,13,14,25]. Metal doping – e.g. by chromium – promotes sp^3 to sp^2 and lowers stress [26]. Zhang and co-workers showed that the I_d/I_g ratio was directly related to the substrate bias [24]. An alternative approach to stress control without metal doping is to alter the substrate bias through the deposition, bias-grading or multilayering with alternate high- and low- bias to produce hard-soft layers, or do produce maximum stiffness at a controlled depth [11, 18, 23]. Duplex surface engineering has been employed to increase the load-carrying capacity of soft metallic substrates. Dong and co-workers reported plasma carburizing of stainless steel to produce a carbon-rich S-phase case layer prior to a multilayer deposition (columnar Cr interlayer, graded Cr/C multilayer, amorphous Cr doped carbon layer) [20], and boost-diffusion oxidation of Ti6Al4V prior to deposition of similar a-C coating system [21].

Improved performance has been shown in indentation tests with relatively sharp spherical indenters, in scratch tests and in pin-on-disk wear tests but for many applications it is also important to evaluate the coating performance under more complex loading conditions, where repetitive impact or impact-sliding may occur. Under repetitive contact conditions the coatings may even show weakening behaviour. Bouzakis and co-workers reported that whilst thin a-C top-layers could improve the fatigue resistance of TiAlN coatings on hard steel, the number of impacts required for total removal of CrN on steel was dramatically reduced by the addition of a a-C:H top layer to the coating system [27]. In impact sliding of DLC coated Ti6Al4V and CoCr the DLC coating reduced the durability due to the formation of hard particles which caused micro-cutting and severe third-body abrasive wear [28].

At the macro-scale coating impact resistance is commonly evaluated in non-depth sensing tests with indenters of WC-Co, hardened steel [29] or silicon nitride [30], typically with radii of 2.5 or 3 mm [30-34] although smaller radii (e.g. around 1 mm) have also been used [35-40]. Although simple in principle, these macro-scale impact tests have certain drawbacks which limit their usefulness. As they are not depth-sensing the exact time at which the coating fails is not clearly defined; it is only possible to say that the coating has survived or failed after the test is ended. The tests are time-consuming and due to the large size of the test probe the response is averaged out over a larger area of the coating surface making it insensitive to e.g. situations where the fatigue behaviour varies across a sample (for example through coating thickness variation or mechanical property variation). The failure criterion itself is somewhat arbitrary [30] with average measures such as failure area at a given number of cycles being used [27]. The coating wear depth at the end of the test has as a failure criterion been used but this requires time-consuming FIB sectioning to deconvolute the coating wear from substrate plasticity [37-38]. Although the fatigue mechanisms can vary with the ratio of coating thickness to the indenter radius [41] the macro-scale tests are necessarily over a limited range of h/R values which are very low. Under these conditions the peak stresses are well into the substrate and the coating contribution to the overall fatigue behaviour may be reduced and the results more strongly influenced by the substrate hardness and toughness as has also been reported in erosion testing under severe conditions [42].

Improved understanding of the evolution of coating damage is possible by nano-impact testing which utilises the depth sensing capability of a nanoindentation system (NanoTest) to perform impact indentation testing at strain rates several orders of magnitude higher than in quasi-static indentation. The high strain rate contact in this test can provide much closer simulation of the performance of coatings systems under highly loaded intermittent contact and the evolution of wear under these conditions. In practice, studies have reported a strong correlation between

coating performance in the nano-impact test and life of coated tools in high speed machining of hard-to-cut materials [43], and in solid particle erosion testing [44]. A cube corner diamond indenter whose geometry induces high contact strain is often chosen as the test probe, as this high contact strain is beneficial in inducing fracture within a short test time. Benefits of assessing coating fatigue resistance with the nano-impact test include:- (i) short duration of the experiments compared to conventional tests allowing rapid screening to evaluate the performance of novel coating compositions (ii) multiple rapid tests possible on single samples (iii) flexibility to alter loading level and severity of impact loading (iv) accurate recording of cycles to failure (v) information on the fatigue failure mechanism.

By changing the applied load and probe geometry in an impact test, it is possible to alter the severity of the test and to move the positions of peak impact-induced stresses relative to the coating-substrate interface. A new micro-impact test capable of applied loads in the micro-range (~ 0.5 -5 N) has recently been developed. The energy supplied per impact is the product of the impact load and accelerating distance [45]. The maximum energy supplied per impact with the micro-impact technique is around 2 orders of magnitude greater than the maximum possible in the nano-impact technique. It retains the intrinsic depth-sensing capability of the nano-impact test enabling the progression of the wear process to be monitored throughout the test, combined with the opportunity to use probes of less sharp geometry. The use of blunter probes prolongs the life of the tip and reduces the requirement of monitoring probe sharpness, simplifying the testing. In this work, we have used the new micro-impact capability to investigate the impact fatigue resistance of a-C:H and a-C films produced by sputter and by hybrid sputter CVD deposition respectively. The coatings were deposited on a hard steel substrate (M42 tool steel) providing enhanced load support. Both of these coating systems have been shown to have high wear resistance in pin-on-disk tests in air and under lubricated conditions [14-17, 19-22]. Carbon-chromium coatings produced by the unbalanced magnetron

sputtering have been reported to have a graphitic structure with no long range order [14-17]. The predominantly sp^2 bonding can impart low stress and improve adhesion, particularly with the addition of chromium to soften and toughen the coatings [46]. The hardness of sputtered a-C is commonly in the range 12-18 GPa although, it is possible to produce significantly harder films if there is no metal doping [15,23,24]. Increasing the sp^3/sp^2 ratio leads to higher hardness but also larger residual stress which causes cracking and/or delamination under high loading applications [22].

The main aims of the study were (i) to use the novel micro-impact test to improve our understanding of the fatigue failure of hard coatings deposited on hard substrates (ii) compare to nano-impact (much higher h/R) and macro-impact (much lower h/R). Mechanistic information obtained by following the evolution of the depth during the test is complemented by SEM, EDX and Raman analysis of the impact craters. By performing micro-scratch tests with the same probe as the micro-impact tests comparative information regarding the severity of the tests was also obtained.

2. Experimental

2.1 Coatings

The two coating systems tested were compositionally graded a-C (Graphit-iC [14-17,45]) and a-C:H (Dymon-iC [16-17]) coatings deposited on M42 tool steel. The amorphous carbon coating Graphit-iC was deposited from solid carbon (graphite) and chromium targets in an industrial closed field unbalanced magnetron sputter ion plating (CFUBMSIP) system. After deposition of a 0.4 μm adhesion promoting Cr layer, a ramp layer was produced by gradually decreasing power on the Cr targets and increasing the power on the carbon targets followed by

Cr doped C top layer. The hydrogenated Dymon-iC was deposited using a Teer hybrid unbalanced magnetron sputter ion plating/PECVD system. A Cr bond layer was followed by a CrC base layer using butane gas, and finally an a-C:H top layer with d.c. bias and RF electrode for supplementary plasma enhancement. The Graphit-iC had a total coating thickness of 2.5 μm and the Dymon-iC a total coating thickness of 2.8 μm . The R_a surface roughness of the coatings determined from line profiles at low load in multi-pass micro-scratch tests (NanoTest Vantage) was 45 nm for Graphit-iC and 34 nm Dymon-iC. Mean values were from five repeats on Dymon-iC and 10 on Graphit-iC.

2.2 Mechanical characterisation

Nano- and micro-scale mechanical characterisation was performed with a NanoTest system (Micro Materials Ltd., Wrexham, UK) with a low load (0-500 mN) head for nanomechanical testing and a high load (0-30 N) head for micromechanical testing. The previously published [47-48] nanomechanical data is summarised in Table 1(a). Due to the high surface roughness the H and E are mean values determined from >60 indentations to 200 nm. The maximum indentation depth of 200 nm is under 10 % of the coating thickness. The choice of 200 nm reflects a compromise to minimise the influence of the high surface roughness and the elastic properties of the substrate on the measured elastic modulus. Previously published nano-impact data are summarised in Table 1(b) [47-48].

Micro-indentation, micro-scratch and micro-impact tests were performed on a NanoTest Vantage (Micro Materials Ltd., Wrexham, UK) using the same spheroconical diamond probe for all the tests. The end radius of this nominally 25 μm probe was determined as 18 μm by spherical indentation testing on fused silica.

Spherical micro-indentation tests were performed over a range of loads up to 3.5 N on Dymon-iC and 12 N on Graphit-iC loading in 20 s, 30 s hold at peak load and 5 s unload, with thermal

drift assessed from a 60 s hold at 90% unloading. Micro-scratch testing to 5 N was performed using a 3-scan procedure. The procedure involved 3 sequential scans, topography-scratch-topography, at 20 $\mu\text{m/s}$, always in the same direction. These were (i) pre-scan: scanning at 0.2 mN over a 2000 μm track (no wear occurs at this load with a 18 μm probe) (ii) progressive load scratch: the load is low (0.2 mN) over the first 200 μm scan then ramping at a constant rate of 55 mN/s to reach 5 N at the end of the scan (iii) post-scan: with the same low load as the pre-scan. 5 scratch tests were done on each sample, with the scratch direction parallel to the machining marks, with adjacent tracks separated by 100 μm . 5 tests were also performed on the Graphit-iC sample oriented with the scratch direction perpendicular to the machining marks. Friction was measured during micro-scratch tests using calibrated tangential force sensors. The critical loads for yield (L_y), cracking (L_{c1}) and total coating failure (L_{c2}) were determined from on-load and residual depth data, friction and confirmed by SEM with EDX. Repetitive scratch tests were performed on Graphit-iC at 1.5 N.

To enable micro-impact tests to be performed, the high load (30 N) head of a NanoTest Vantage was extended below the indenter position. This adapted loading head was actuated with a large electromagnet capable of pulling the probe at least 50 μm away from the sample surface. The impact energy and effective impact force can be controlled by varying the static load and the accelerating distance [45]. In this study repeat micro-impact tests were performed at 0.5-2.0 N with the accelerating distance kept constant at 40 microns from the initial coating surface. The test duration was 300 s with 1 impact every 4 s, resulting in 75 impacts in total. There were 3 repeats at each load which were separated by 100 μm . Three 1200 s tests at 2 N were also performed on the Graphit-iC coating. The indenter area function did not change after the impact tests. Raman spectra were acquired with an inVia-reflex Raman spectrometer (Renishaw), with Ar^+ 488 nm laser. Spectra were analysed to assess the relative intensity of the D- and G-peaks, (I_d/I_g), FWHM and G-peak position of the unworn coatings and in the centre of the impact

craters which were also imaged by SEM with EDX. The scanning range was from 1000 cm^{-1} to 2000 cm^{-1} with a resolution of 1 cm^{-1} . Before scanning the light spot was focused in the middle of the impact craters and three repeat measurements performed for the different craters at each load. The laser spot size was under 0.5 μm .

3. Results

3.1 Microindentation and micro-scratch

The spherical micro-indentation tests confirmed the coatings are less stiff than the steel substrate/other layers and the composite measured modulus increased towards expected value for the steel substrate as the depth increased. The critical loads for yield, cracking and total film failure (L_y , L_{c1} , L_{c2} respectively) are shown in Table 2. The critical loads were higher for the Graphit-iC coating. SEM images of scratch tracks are shown in figure 1. There were isolated failure events on the Graphit-iC which did not rapidly lead to a complete L_{c2} failure but on Dymon-iC these events were soon followed by total film failure. EDX analysis showed that the initial failure on Dymon-iC involved exposure of Cr whilst the isolated and total failure events on Graphit-iC resulted in substrate exposure. Repetitive tests on Graphit-iC at 1.5 N (a load well below L_{c1}) showed that coating failure occurred progressively over a greater area of the scratch track at an on-load depth a few hundred nm below that required for cracking in the ramped test.

3.2 Micro-impact

Figure 2 shows typical impact vs. time data at 0.5-2 N for (a) Dymon-iC and (b) Graphit-iC. On Dymon-iC after the first few impacts there is little change in depth with subsequent impacts at 0.5 N but at higher loads the curves are characterised by inflexions (onset of more severe failure) where the rate of damage is greater after (at ~230 s at 0.75 N, ~150 s at 1 N, ~70 s at

1.5 N and ~30 s at 2 N). They are absent on Graphit-iC over the entire range of applied load and the depth becomes approximately constant after a number of impacts (plateau depth). The number of impacts required to reach this plateau depth increases at higher load, which can be more clearly seen in the initial 0-60 s of the tests on Graphit-iC (figure 2(c)). The number of impacts to reach plateau depth (on both coatings) and number of impacts to failure of the Dymon-iC coating (figure 2(d)) show completely different dependencies on the applied load. The mean initial impact depth and depth at the end of the 300 s tests are shown in figure 3(a,b). The depth data in this figure are under-load, so include the elastic, plastic/fracture deformation, after removing the contribution from the compliance of the test frame.

SEM reveals differences in behaviour at the lowest applied load. Circumferential cracks form on both samples (figure 4a,b) at 0.5 N but on Dymon-iC there is more than one crack and they are more continuous forming partial and complete concentric rings but on Graphit-iC only a single faint circumferential crack is formed whose direction is influenced by the coating surface morphology. On Graphit-iC this cracking becomes more established at 0.75-1.25 N and multiple short concentric cracks become clear at 1.5 N. From 1.75 N short radial cracks, extending up to 5-10 μm are observed which are deflected by the coating surface morphology (figure 4(c)). At >0.5 N on Dymon-iC there is dramatic coating failure (figure 4(d)) which extends further laterally as the load increases, with wear debris observed in the centre of impact crater. EDX analysis of impact craters on Dymon-iC showed the presence of Cr in a region at the edge of the impact crater in one test at 0.5 N, but this was absent in the other tests at this load. In all the tests at higher load (0.75-2 N) there was significant Cr and O around the periphery of the impact crater, with reduction in C intensity but no substrate exposure. Chipped regions extending out from the impact crater showed the presence of Cr and C but with much less oxygen than around the periphery (4(d)).

Raman spectra from the unmodified coatings and in the centre of the impact craters are shown in figure 5 (a,b). The peak intensity ratio of the D-band to that of the G-band (I_d/I_g) was 2.1 for Dymon-iC and 3.8 for Graphit-iC. The spectra are almost completely unchanged after the impact tests on Graphit-iC but differences in peak intensity ratio, G-peak position and FWHM were found on Dymon-iC.

4. Discussion

4.1 Correlation between coating mechanical properties and wear resistance

The nanoindentation data summarised in Table 1 show that both coatings have broadly similar hardness and elastic modulus but since the harder film (Dymon-iC) is lower modulus significant differences in H/E and H^3/E^2 . The values of hardness are low compared to some a-C and a-C:H films but are close to reported values on other Graphit-iC and Dymon-iC films deposited by CFUBMSIP [16,17,20,21].

The analysis of the Raman spectra shows that I_d/I_g in the hydrogen-free Graphit-iC is 3.8 and in the hydrogenated Dymon-iC it is 2.1. The lower I_d/I_g with increased hydrogen content in the films is in agreement with previous reports by hybrid sputter/CVD [22] and RF-PECVD [49]. Zhang and co-workers [50] showed that the I_d/I_g and G-peak position were strongly correlated with the sp^2/sp^3 ratio measured from electron energy loss spectroscopy (EELS) analysis. The high I_d/I_g in Graphit-iC reflects the very high sp^2 fraction in this coating, as has been reported previously, with Zeng and co-workers reporting that I_d/I_g could reach 5-9 in sputter deposited a-C coatings [22].

Differences in mechanical properties influence the coating performance in different types of wear test. In general very high sp^3/sp^2 bonding in a-C:H coatings confers higher hardness and

H/E , which at a given load results in closer to elastic contact and lower rates of wear in pin-on-disk tests but can lead to reduced durability in highly loaded contacts. The Dymon-iC film has higher I_d/I_g than the majority of hard DLC films and this results in moderate hardness (17 GPa) and very low wear rate in pin-on-disk tests even at 80 N [16-17]. a-C coatings have shown excellent performance in a range of highly loaded applications [4,23,24,27,30]. Although the hardness of many of these coatings was ~14 GPa high wear resistance was also observed for harder and softer films.

In scratch tests softer a-C coatings tend to show higher critical load than harder a-C and a-C:H coatings [22, 25, 51]. Schwarzer and co-workers have shown that the maximum von Mises stresses in the conventional macro-scale scratch test with a 200 μm diamond can be far into the substrate before the coatings fail and “dimensioning” the test by choosing a suitable indenter geometry to position the peak stresses closer to the interfaces may be more appropriate [52]. To emphasize the importance of the load carrying capacity of the substrate on scratch test data, Wang and co-workers have shown that critical width of the scratch groove at peak load did not vary with substrate hardness whilst the substrate hardness influenced the critical load more than the coating composition [53,54].

Micro-scratch tests on various carbon coatings with a 25 μm end radius probe have shown critical loads (L_y , L_{c1} , L_{c2}) correlated to the coating mechanical properties [55]. Although the micro-scratch data with the $R = 18 \mu\text{m}$ probe are scattered due to surface roughness, the slightly higher L_y on Dymon-iC may be connected to its H^3/E^2 and its higher thickness shielding the substrate from the stress field of the contact [7]. Analytical stress field modelling suggests that although the position of peak von Mises stress is within the coating top layer at L_y , the stress is below the coating yield stress and yield occurs by the substrate yield stress being exceeded at (and below) the interface. In the progressive and repetitive scratch tests the Graphit-iC coating

appeared more damage tolerant. Failure of isolated regions of the Graphit-iC coating in the progressive load test did not immediately lead to total failure whilst in the repetitive test failure occurred by progressive removal of the coating with each cycle rather than a dramatic debonding. This type of failure is consistent with a tougher coating with higher plasticity (lower H/E). Zhang and co-workers have equated L_{c1} with the resistance to the initiation of cracks and $(L_{c2}-L_{c1})$ as a measure of the toughness (L_{c2} = load for total failure) [56-58]. They defined a parameter representing resistance to crack initiation and also propagation (later called scratch toughness) as the sum of the lower critical load and the additional load to reach L_{c2} (i.e. scratch toughness = $L_{c1}(L_{c2}-L_{c1})$). The scratch toughness was $(0.3 \pm 0.1) \text{ N}^2$ on Dymon-iC and $(1.9 \pm 0.5) \text{ N}^2$ on Graphit-iC.

The Dymon-iC is more susceptible to cracking in the micro-impact test than the graded a-C coating Graphit-iC. Although improved wear resistance has been reported for coatings with high H/E , since this is related to the elastic strain-to-break [59-60], under the severe conditions in the micro-impact test the greater susceptibility to cracking of Dymon-iC outweighs benefit on enhanced load-carrying capacity (through higher H/E) and causes failures of the top layers.

The a-C coating showed significantly improved impact resistance compared to the a-C:H coating, despite its lower hardness and significantly lower H/E . Under highly loaded conditions there may be benefit in designing coatings with compositional grading, for efficient stress transfer to substrate and some measure of plasticity for stress relief. The smaller difference in hardness between the coating and substrate in Graphit-iC helps the coating to accommodate plastic deformation of the substrate without cracking [61]. In automotive engine applications [32,62] involving a combination of load support and resistance to fatigue optimum lifetime of coated components may be achieved by designing the coating system to combine these properties rather than by solely aiming to maximise coating hardness as this may be accompanied by brittle fracture and higher wear.

Using the same probe for the impact and scratch tests provides an opportunity to compare the severity of the two types of test. Dramatic failure of the Dymon-iC coating in the scratch load occurs at an applied load 1.2 N whilst in the impact test the coil force required was 0.75 N resulting in a dynamic force of 3.1 N. When comparing on-load depth data (including the elastic, plastic/fracture deformation, but after removing the contribution from the compliance of the test frame) it can be seen that the depths at failure are smaller in the micro-scratch test than the impact test which presumably reflects the importance of shear forces in the scratch test.

4.2 Impact fatigue mechanisms

A clear advantage of depth-sensing in the micro-impact test is that the damage progression with subsequent impacts can be monitored and the exact time-to-failure known. Figure 2 clearly shows that the number of impacts to reach plateau depth (on both coatings) and number of impacts to failure of the Dymon-iC coating exhibit very different dependencies on the applied load.

In impact tests of DLC at 70-240 N with a steel pin of 1 mm radius, Abdollah and co-workers determined a deformation-wear transition map involving three stages to the evolution of impact wear:- (1) plastic deformation of the substrate without coating wear (2) suppression of plastic deformation of substrate (3) wear of the DLC coating, with the transitions between regions being dependent on the normal impact load and the number of impact cycles [37]. Although the mechanism at the micro-scale when impacted with the 18 μm probe has similar features the number of impacts required for the transition between regions 1 and 2 (figure 2(c)) shows an opposite trend to that reported at larger contact size which may be due to the greater accuracy in the depth-sensing micro-impact test.

To better understand the fatigue mechanism in the micro-impact test, the evolution of mean pressure during the test has been calculated from the dynamic impact force and the contact area under load. The impact force is larger than the quasi-static coil force (applied load). Although the impact force can be calculated from impact vs. time plots in this work a different approach was adopted since hard carbon coatings are not particularly rate sensitive. For both coatings the loading curves in spherical micro-indentation superimposed over a $\times 100$ change in loading rate. The on-load depth in the impact test was equated with same on-load depth in the microindentation test. The quasi-static load necessary to produce this deformation was then taken as the actual force in the dynamic impact. The residual depth was estimated from a calibration curve of the degree of elastic recovery for a given depth under load. Data on either coating can be used since although differences in mechanical properties were observed in the nanoindentation tests with the sharp Berkovich indenter the load-displacement curves with the spherical indenter at the micro-scale and the initial (pre-impact) depth in the impact tests were essentially identical on either coating as they were increasing dominated by the substrate properties.

Hertzian calculations show that on initial impact the mean contact pressure is around 13 GPa on both coatings. The initial impact depth is greater for the Dymon-iC film, presumably reflecting more cracking (SEM from end of the tests show that cracking is more developed on Dymon-iC at 500 mN). The contact pressure gradually reduces with each subsequent impact to reach the plateau contact pressure. In macro-scale tests where the ratio h/R is very low so that the presence of the thin hard coating barely influences the elastoplastic deformation of the steel substrate the mean pressure is close to $1.1 Y$ [37].

In tests at the micro-scale the mean pressure in this region (region 2) is to a large extent controlled by substrate yield stress. Hertzian calculations provide a value of ~ 11 GPa for the mean contact pressure. The method has been used in nano-impact tests on silicon, with good

agreement between the mean contact pressure and $1.1 Y$ [63]. The substrate yield stress can be estimated from the hardness and H/E which influences the constraint factor H/Y [64]. M42 is a very hard tool steel, with nanoindentation hardness of 12 GPa with $H/Y \sim 2.5$ the yield stress is estimated at ~ 4.8 GPa. Several factors appear to be responsible for the calculated mean pressure being higher than $1.1 Y$ at this scale including (i) with the smaller probe there is more influence from the harder, higher yield stress coatings (ii) a size effect in yield stress (iii) work hardening with repetitive impact (iv) cracking reducing contact pressure (v) deviations from Hertzian conditions (vi) elastic recovery on unloading and re-yielding on next impact.

Hertzian elastic analysis predicts cracks form at the edge of the contact (at the contact radius a). When plasticity occurs cracks form outside the contact at a distance up to $2a$. [41,65] Michler and Blank have reported that when $3.3 \mu\text{m}$ DLC coatings on steel were indented by a $10 \mu\text{m}$ probe ($h/R = 0.33$) circumferential cracks form at up to $2a$ [41]. SEM shows that for these coatings ($h/R = 0.14\text{-}0.16$) cracks form at $\sim 1.5\text{-}1.8 a$. On Dymon-iC there are multiple ring cracks at 500 mN but at the same load on Graphit-iC a single crack appearing to follow the surface morphology (related to machining marks on the steel prior to deposition) was found.

Although a plateau depth was observed for both coatings at 0.5 N when the coatings were tested at 0.75 N (figure 6) it can be seen that a plateau depth was not observed for Dymon-iC. The coating is more susceptible to cracking with small scale cracks joining up resulting in gradually increasing depth due to material removal. In contrast on Graphit-iC there were no cracks within central zone and the depth stabilises. These differences are supported by Raman spectra inside the impact craters, as discussed below.

The regions of highest stresses are at the periphery of the impact crater. In tests on Dymon-iC at ≥ 0.75 N the EDX in this region shows chromium and oxygen but little remaining carbon and no Fe from the substrate. The EDX spectra show that around the periphery the a-C:H top layer

and CrC base layer are removed and the Cr bond layer is exposed. Although there was significant chipping damage around the impact craters the absence of Fe from the substrate shows the strong bonding between the Cr adhesion layer and the steel is maintained. The presence of more oxygen in the wear debris in the highly loaded region at the periphery of the impact crater and little/no oxygen incorporation in the chipped regions extending beyond this could suggest a tribochemical component to the degradation process, or that simply that chromium is more susceptible to oxidation than when present as CrC.

sp^3 to sp^2 phase transformations and graphitisation in carbon films have been well studied in sliding contact but with a couple of notable exceptions they have not been investigated in impact [37,39]. Abdollah et al reported that the G-peak of wear debris at the edge of an impact crater (10^4 cycles at 240 N with a 1 mm steel pin) shifted to higher frequency compared to as-deposited hydrogenated DLC due to breaking of tetrahedral bonds and increasing sp^2 bonding [37]. Decreasing FWHM was due to increasing dominance of crystallites. Figure 7 shows the variation in I_d/I_g , FWHM and G-peak position with impact load in the micro-impact test. On the hydrogenated DLC, Dymon-iC similar trends in the centre of the impact craters were observed. Cracking is correlated with increasing sp^2/sp^3 . However, on an a-C coating with 25 GPa hardness and a low I_d/I_g of 0.63 it was reported that with increasing number of impacts at 70-240 N the I_d/I_g decreased to 0.47-0.49 after 10^5 impacts and the FWHM of the G-peak increased which was interpreted as work-hardening. [39]. On Graphit-iC there was little clear change in the I_d/I_g ratio after 300 s, although it did decrease after 1200 s (300 impacts) at 2 N. Although the Graphit-iC and Dymon-iC films had significantly higher I_d/I_g than the a-C and DLC coatings tested by Abdollah and co-workers nevertheless there are some similarities in behaviour with decreasing I_d/I_g on repetitive impact for the a-C coatings and damage on a-C:H causing increasing I_d/I_g .

4.3 Influence of probe radius - nano- vs. micro-impact

The amount of plastic deformation, and hence coating bending and tensile stresses developing at the edge of the contact is a function of the applied load (hence impact energy) and indenter radius. Increasing the applied load results in greater substrate plasticity and higher tensile stresses and failure becomes more severe and after fewer impacts. Michler and Blank have shown using finite element analysis (FEA) that changing the ratio between coating thickness h and indenter radius R (h/R) can alter the dominant failure mechanisms [41]. When the ratio is very low, as is the case of the majority of published non-depth sensing impact tests with probes with ~ 3 mm radii, the substrate plasticity can be reduced (depending on load) and the mechanical properties of the film itself do not influence the elasto-plastic deformation of the substrate. Under these conditions a high-cycle coating (or substrate) fatigue process may occur, with highest tensile stresses very close to the edge of the contact and blistering inside the impact zone. In impact tests with much lower h/R detailed investigation of the fatigue wear process has shown that isolated delamination is preceded by blistering [35-36].

The h/R ratio is completely different in the micro- and nano-impact tests. The cube corner indenter used in nano-impact has a very sharp end radius so it is effectively more pyramidal at the depths reached in the nano-impact tests making it difficult to assign an exact effective radius. However, if the effective radius for the cube corner indenter is at least a few hundred nm for larger penetration depths, then h/R is of the order of 1-10 in the nano-impact tests and ~ 0.15 in the micro-scale tests. In the nano-impact tests with a cube corner diamond indenter reported in [47-48] Graphit-iC was significantly more durable than Dymon-iC, with much longer time to failure and smaller changes in depth on failure. These differences between the two coatings increased with load as chipping/ring cracks were more extensive at higher load on Dymon-iC. Similar trends were found in the micro-impact tests but as it was not possible to obtain abrupt changes in depth within the 300 s tests on Graphit-iC three further 1200 s tests were carried out at 2 N. The tests showed that in the apparent “plateau” region the actual wear

depth was not quite constant but increased very slowly at a rate of ~1-1.5 nm per impact, although there were no abrupt changes in depth (figure 8). Raman analysis showed a decrease in I_d/I_g consistent with higher sp^3 and work hardening. The very gradual increase in depth is not necessarily a result of the Graphit-iC wearing away but more potentially a fatigue wear process in the M42 substrate, for example, involving carbide fracture. In contrasting failures induced by sharp probe impact at 5 or 15 mN [47,48] with higher load spherical impact, it can be seen that at the nano-scale the failure process typically takes place over a shorter number of cycles whilst at the micro-scale it proceeds more gradually.

4.4 Micro-impact – current status and opportunities for test method development

The new micro-scale impact test fills a large gap in terms of h/R between macro-scale and nano-scale impact tests and has distinct potential advantages over both. In comparison to macro-scale tests it is advantageous for coating screening campaigns to be able to test a large number of coatings in a short space of time and the rapid micro (and nano) impact tests make this possible whilst providing additional information regarding the evolution of the impact wear process.

The micro-impact test retains the intrinsic depth-sensing capability of the nano-impact test enabling the progression of the impact fatigue process to be monitored throughout the test. Since significantly higher impact energies are obtained than in the nano-impact test it is possible to cause rapid coating failure with larger radii indenters. The tests were performed with a diamond probe with 18 μm end radius but significantly sharper or blunter geometries are also possible to change h/R and investigate different fatigue mechanisms. Diamond was chosen as (1) it could be used for the micro-indentation and micro-scratch experiments (2) it showed no probe wear, but other probe materials are possible e.g. to simulate specific application conditions. When other materials have been used in macro-impact tests specific

tribochemical interaction has been reported to be a complicating factor leading to (i) on-going probe wear (ii) transfer layer formation and subsequent break-up resulting in formation of micro-scale debris which can enhance wear rate [31]. The tests described here were stopped after a set time (i.e. pre-defined number of impacts). However, as the probe depth is monitored throughout the test, with software modification it will be possible to stop the test immediately after a failure event occurs so that subsequent damage does not complicate interpretation of the failure mechanism.

In the current study, ring-cracking was observed on both samples at the lowest test force, and the investigation focussed on crack propagation mechanisms after formation of ring crack(s). Single micro-impacts can also be set up, and could be used in lower force tests (and/or different probe geometries) to determine the minimum loads required for the onset of ring cracking (i.e. to study crack initiation). The described tests were performed at 25 °C with normal (90°) impact but it is also possible to perform angled impact and/or elevated temperature tests with the test setup. Angled impact increases the sensitivity to adhesion [66] and also could be more representative of contact occurring in gears [30] or automotive engine applications such as cam-tappet in valve train [4], whilst the tribology of DLC can be strongly dependent on temperature [67].

5. Conclusions

The new micro-scale impact test fills a large gap in terms of the ratio between coating thickness and the radius of the impact probe (h/R) between macro-scale and nano-scale impact tests. In the micro-impact test the Dymon-iC shows greater susceptibility to cracking than the graded a-C coating Graphit-iC. Raman spectra show marked differences in I_d/I_g ratio consistent with their sp^2/sp^3 bonding and mechanical properties. Spectra taken from the centre of the impact

craters show an increase in the I_d/I_g ratio for Dymon-iC due to cracking whilst on Graphit-iC the initially very high ratio is unchanged in 300 s tests and decreases only slightly after 1200 s tests at 2 N. The graded a-C coating Graphit-iC shows better performance in micro-scale scratch tests. In highly loaded mechanical contact applications requiring a combination of load support and resistance to fatigue optimum lifetime of coated components may be achieved by designing the coating system to combine these properties rather than by solely aiming to maximise coating hardness as this may be accompanied by brittle fracture and higher wear.

6. Acknowledgements

The funding to develop the novel micro-impact test technique through the Innovate UK Project No: 132369 – “Nano-to Micro-Impact Testing: An in-situ test for UK SEAC sector” is gratefully acknowledged. The authors gratefully acknowledge the financial support from the program of China Scholarships Council (CSC, No. 201706090126). Nick Pickford and Dr Stephen Goodes (both Micro Materials Ltd.) are acknowledged for modifying the NanoTest hardware and software respectively to develop the new micro-impact capability. Dr Nathalie Renevier (UCLAN) is thanked for supplying the coatings and for many useful and stimulating discussions.

7. References

1. A. Erdemir, C. Donnet, Tribology of diamond-like carbon films: recent progress and future prospects, J. Phys. D: Appl. Phys. 39 (2006) R311-R327.

2. U. Depner-Miller, J. Ellermeier, H. Scheerer, M. Oechsner, K. Bobzin, N. Bagcivan, T. Brögelmann, R. Weiss, K. Durst and C. Schmid, Influence of application technology on the erosion resistance of DLC coatings, *Surf. Coat. Technol.* 237 (2013) 284-291.
3. W. Tillmann, N.F.L. Dias, D. Stangier, Tribo-mechanical properties of CrC-a-C thin films sequentially deposited by HiPIMS and mfMS, *Surf. Coat. Technol.* 335 (2018) 173-180.
4. S.D.A. Lawes, S.V. Hainsworth, M.E. Fitzpatrick, Impact wear testing of diamond-like carbon films for engine valve-tappet surfaces, *Wear* 268 (2010) 1303-1308.
5. A.C. Ferrari, J. Robertson, Raman spectroscopy of amorphous, nanostructured, diamond-like carbon, and nanodiamond, *Phil. Trans. R. Soc. Lond. A* 362 (2004) 2477-2512.
6. D. Bernoulli, A. Rico, A. Wyss, K. Thorwarth, J.P. Best, R. Hauert, R. Spolenak, Improved contact damage resistance of hydrogenated diamond-like carbon (DLC) with a ductile α -Ta interlayer, *Diam. Relat. Mater.* 58 (2015) 78-83.
7. D. Bernoulli, A. Wyss, R. Raghavan, K. Thorwarth, R. Hauert, R. Spolenak, Contact damage of hard and brittle thin films on ductile metallic substrates: an analysis of diamond-like carbon on titanium substrates, *J. Mater. Sci.* 50 (2015) 2779-2787.
8. J. Jiang and R.D. Arnell, On the running-in behaviour of diamond-like carbon coatings under the ball-on-disk contact geometry, *Wear* 217 (1998) 190-199.
9. Z.-H. Xie, R. Singh, A. Bendavid, P.J. Martin, P.R. Munroe, M. Hoffman, Contact damage evolution in a diamond-like carbon (DLC) coating on a stainless steel substrate, *Thin Solid Films* 515 (2007) 3196-3201.
10. M. Weidner, O. Borrero-López, M. Hoffman, A. Bendavid, P.J. Martin, Effect of substrate roughness on the contact damage on thin brittle films on brittle substrates, *Thin Solid Films* 518 (2010) 5242-5248.

11. O. Borrero-López, M. Hoffman, A. Bendavid, P.J. Martin, Substrate effects on the mechanical properties and contact damage of diamond-like carbon films, *Diam. Relat. Mater.* 19 (2010) 1273-1280.
12. R.K. Singh, Z. Zhou, L.K.Y. Li, P. Munroe, M. Hoffman, Z. Xie, Design of functionally graded carbon coatings against contact damage, *Thin Solid Films* 518 (2010) 5769-5776.
13. M. Antonov, I. Hussainova, F. Sergejev, P. Kulu, A. Gregor, Assessment of gradient and nanogradient PVD coatings under erosive, abrasive and impact wear conditions, *Wear* 267 (2009) 898-906.
14. S. Yang, X. Li, N.M. Renevier, D.G. Teer, Tribological properties and wear mechanism of sputtered C/Cr coating, *Surf. Coat. Technol.* 142-144 (2001) 85-93.
15. D.G. Teer, New solid lubricant coatings, *Wear* 251 (2001) 1068-1074.
16. J. Stallard, D.G. Teer, A study of the tribological behaviour of CrN, Graphit-iC and Dymon-iC coatings under oil lubrication, *Surf. Coat. Technol.* 188-189 (2004) 525-529.
17. J. Stallard, D. Mercks, M. Jarratt, D.G. Teer, P.H. Shipway, A study of the tribological behaviour of three carbon-based coatings, tested in air, water and oil environments at high loads, *Surf. Coat. Technol.* 177-178 (2004) 545-551.
18. Y. Lin, A.W. Zia, Z. Zhou, P.W. Shum, K.Y. Li, Development of diamond-like carbon (DLC) coatings with alternate soft and hard multilayer architecture for enhancing wear performance at high contact stress, *Surf. Coat. Technol.* 320 (2017) 7-12.
19. Y. Wang, J. Pu, J. Wang, J. Li, J. Chen, Q. Xue, Interlayer design for the graphite-like carbon film with high load-bearing capacity under sliding friction condition in water, *Appl. Surf. Sci.* 311 (2014) 816-824.

20. W. Wu, X. li, J. Chen, H. Dong, Design and characterisation of an advanced duplex system based on carbon S-phase case and GiC coatings for austenitic stainless steel, *Surf. Coat. Technol.* 203 (2009) 1273-280.
21. Z.X. Zhang, H. Dong, T. Bell, The load bearing capacity of hydrogen-free Cr-DLC coatings on deep-case oxygen hardened Ti6Al4V, *Surf. Coat. Technol.* 200 (2006) 5237-5244.
22. X.T. Zeng, S. Zhang, X.Z. Ding, D.G. Teer, Comparison of three types of carbon composite coating with exceptional load-bearing capacity and high wear resistance, *Thin Solid Films* 420-421 (2002) 366-370.
23. S. Zhang, X.L. Bui, Y. Fu, D.L. Butler, H. Du, Bias-graded deposition of diamond-like carbon for tribological applications, *Diam. Relat. Mater.* 13 (2004) 867-871.
24. S. Zhang, X.L. Bui, X.T. Zeng, X. Li, Towards high adherent and tough a-C coatings, *Thin Solid Films* 482 (2005) 138-144.
25. M. Diesselberg, H.-R. Stock, P. Mayr, Friction and wear behaviour of PVD chromium nitride supported carbon coatings, *Surf. Coat. Technol.* 188-189 (2004) 612-616.
26. C.W. Zou, H.J. Wang, L. Feng, S.W. Xue, Effects of Cr concentrations on the microstructure, hardness, and temperature-dependent tribological properties of Cr-DLC coatings, *Appl. Surf. Sci.* 286 (2013) 137-141.
27. K.-D. Bouzakis, A. Siganos, T. Leyendecker and G. Erkens, Thin hard coatings fracture propagation during the impact test, *Thin Solid Films* 460 (2004) 181-189.
28. Y. Chen, J.-M. Wu, X. Nie, S. Yu, Study on failure mechanisms of DLC coated Ti6Al4V and CoCr under cyclic high combined contact stress, *J. Alloys Compd.* 688 (2016) 964-973.

29. S. Lamri, C. Langlade, G. Kermouche, Damage phenomena of thin hard coatings submitted to repeated impacts: influence of the substrate and film properties, *Mater. Sci. Eng. A* 560 (2013) 296-305.
30. E.S. Zanoria, L.E. Seitzman, Characterisation of thin metallurgical coating systems by repetitive inclined impact test in dry condition, *Surf. Coat. Technol.* 182 (2004) 161-170.
31. J.L. Mo, M.H. Zhu, A. Leyland, A. Matthews, Impact wear and abrasion resistance of CrN, AlCrN and AlTiN PVD coatings, *Surf. Coat. Technol.* 215 (2013) 170-177.
32. C.P.O. Treutler, Industrial use of plasma-deposited coatings for components of automotive fuel injection systems, *Surf. Coat. Technol.* 200 (2005) 1969-1975.
33. M.D. Bao, X.D. Zhu, J.W. He, Evaluation of the toughness of hard coatings, *Surf. Eng.* 22 (2006) 11-14.
34. X. Zhu, H. Dou, Z. Ban, Y. Liu, J. He, Repeated impact test for characterisation of hard coatings, *Surf. Coat. Technol.* 201 (2007) 5493-5497.
35. F. Ledrappier, C. Langlade, A.-B. Vannes, Y. Gachon, Damage phenomena observed on PVD coatings subjected to repeated impact tests, *Plasma Process. Polym.* 4 (2007) 5835-5839.
36. F. Ledrappier, C. Langlade, Y. Gachon, A.-B. Vannes, Blistering and spalling of thin hard coatings submitted to repeated impacts, *Surf. Coat. Technol.* 202 (2008) 1789-1796.
37. M.F.B. Abdollah, Y. Yamaguchi, T. Akao, N. Inayoshi, N. Miyamoto, T. Tokoroyama, N. Umehara, Deformation-wear transition map of DLC coating under cyclic impact loading, *Wear* 274-275 (2012) 435-441.

38. M.F.B. Abdollah, Y. Yamaguchi, T. Akao, N. Inayoshi, T. Tokoroyama, N. Umehara, The effect of maximum normal impact load, absorbed energy, and contact impulse, on the impact crater volume/depth of DLC coating, *Tribology Online* 6 (2011) 257-264.
39. M.F.B. Abdollah, Y. Yamaguchi, T. Akao, N. Inayoshi, N. Umehara, T. Tokoroyama, Phase transformation studies on the a-C coating under repetitive impacts, *Surf. Coat. Technol.* 205 (2010) 625-631.
40. F. Löffler, Methods to investigate mechanical properties of coatings, *Thin Solid Films* 339 (1999) 181-186.
41. J. Michler, E. Blank, Analysis of coating fracture and substrate plasticity induced by spherical indentors: diamond and diamond-like carbon layers on steel substrates, *Thin Solid Films* 381 (2001) 119-134.
42. M. Bromark, P. Hedenqvist, S. Hogmark, The influence of substrate material on the erosion resistance of TiN coated steels, *Wear* 186-187 (1995) 189-194.
43. K.-D. Bouzakis, F.Flocke, G. Skordaris, E. Bouzakis, S. Geradis, G. Katirtzoglou and S. Makrimalakis, Influence of dry micro-blasting grain quality on wear behaviour of TiAlN coated tools, *Wear* 271 (2011) 783-791.
44. L. Venkatesh, S.B. Pitchuka, G. Sivakumar, R.C. Gundakaram, S.V. Joshi, Microstructural response of various chromium carbide coatings to erosion and nano impact testing, *Wear* 386-387 (2017) 72-79.
45. C. Zehnder, J.-N. Peltzer, J.S.K.-L. Gibson, S. Korte-Kerzel, High strain rate testing at the nano-scale: a proposed methodology for impact nanoindentation, *Mater. Design.* 151 (2018) 17-28.
46. A.J. Gant, M.G. Gee, L.P. Orkney, The wear and friction behaviour of engineering coatings in ambient air and dry nitrogen, *Wear* 271 (2011) 2164-2175.

47. B.D. Beake and J.F. Smith, Nano-impact testing – an effective tool for assessing the resistance of advanced wear-resistant coatings to fatigue failure and delamination, *Surf Coat Technol* 188-189C (2004) 594.
48. B.D. Beake, Evaluation of the fracture resistance of DLC coatings on tool steel under dynamic loading, *Surf Coat Technol* 198 (2005) 90.
49. Y.-R. Jeng, P.-C. Tsai, K.-T. Wu, Y.-M. Wang, F. C.-N. Hong, S.-M. Huang, K.-C. Chen, Effect of feed gas composition effects on the nanotribological properties of diamond-like carbon films, *Thin Solid Films* 529 (2013) 301-305.
50. S. Zhang, X.T. Zeng, H. Xie, P. Hing, A phenomenological approach for the Id/Ig ratio and sp³ fraction of magnetron sputtered a-C films, *Surf. Coat. Technol.* 123 (2000) 256-260.
51. Z. Li, X. Guan, Y. Wang, J. Li, X. Cheng, X. Lu, L. Wang, Q. Xue, Comparative study on the load carrying capacities of DLC, GLC and CrN coatings under sliding friction condition in different environments, *Surf. Coat. Technol.* 321 (2017) 350-357.
52. N. Schwarzer, Q.-H. Duong, N. Bierwisch, G. Favaro, M. Fuchs, P. Kempe, B. Widrig and J. Ramm, Optimisation of the scratch test for specific coating designs, *Surf. Coat. Technol.*, 206 (2011) 1327-1335.
53. C.T. Wang, A. Escudeiro, T. Polcar, A. Cavaleiro, R.J.K. Wood, N. Gao, T.G. Langdon, Indentation and scratch testing of DLC-Zr coatings on ultrafine-grained titanium processed by high pressure torsion, *Wear* 306 (2013) 304-310.
54. C.T. Wang, T.J. Hamada, A. Laukkanen, H. Ronkainen, K. Holmberg, N. Gao, R.J.K. Wood, T.G. Langdon, An investigation into the effect of substrate on the load-bearing capacity of thin hard coatings, *J. Mater. Sci* 51 (2016) 4390-4398.

55. B.D. Beake, T.W. Liskiewicz, V.M. Vishnyakov and M.I. Davies, Development of DLC coating architectures for demanding functional surface applications through nano- and micro-mechanical testing, *Surf. Coat. Technol.* 284 (2015) 334-343.
56. S. Zhang, D. Sun, Y. Fu and H. Du, Effect of sputtering target power on microstructure and mechanical properties of nanocomposite nc-TiN/a-SiN_x thin films, *Thin Solid Films*, 447–8 (2004) 462-467.
57. S. Zhang, D. Sun, Y. Fu and H. Du, Toughness measurement of thin films: a critical review, *Surf. Coat. Technol.*, 198 (2005) 74-84.
58. Y.X. Wang and S. Zhang, Toward hard yet tough ceramic coatings, *Surf. Coat. Technol.* 258 (2014) 1-16.
59. A. Leyland and A. Matthews, On the significance of the H/E ratio in wear control: a nanocomposite coating approach to optimised tribological behaviour *Wear* 246, (2000) 1-11.
60. A. Leyland and A. Matthews, Design criteria for wear-resistant nanostructured glassy-metal coatings, *Surf. Coat. Technol.*, 177-178 (2004) 317-324.
61. E. Bousser, M. Benkahoul, L. Martinu and J.E. Klemberg-Sapieha, Effect of microstructure on the erosion resistance of Cr-Si-N coatings, *Surf. Coat. Technol.* 203 (2008) 776-780.
62. R. Gåhlin, M. Larsson, P. Hedenqvist, Me-C:H coatings in motor vehicles, *Wear* 249 (2001) 302-309.
63. B.D. Beake, T.W. Liskiewicz, X. Shi, J. Chen, in preparation.
64. A. Clausner, F. Richter, Determination of yield stress from nano-indentation experiments, *Eur. J. Mech. A/Solids* 51 (2015) 11-20.
65. C.J. Studman, J.E. Field, The indentation behaviour of hard metals, *J. Phys. D: Appl. Phys.* 9 (1976) 857-867.

66. K.-D. Bouzakis, P. Charalampous, G. Skordaris, F. Dimofte, N.M. Ene, R. Ehinger, S. Gardner, B.S. Modrzejewski and J.R. Fetty, Fatigue and adhesion characterisation of DLC coatings on steel substrates by perpendicular and inclined impact tests, *Surf. Coat. Technol.* 275 (2015) 207-213.
67. J. Veverkova, S.V. Hainsworth, Effect of temperature and counterface on the tribological performance of W-DLC on a steel substrate, *Wear* 264 (2008) 518-525.

Tables

Table 1 (a) Nanoindentation data

| | H/GPa | E/GPa | H/E | $H^3/E^2 (\text{GPa})$ |
|------------|----------------|----------------|-------|------------------------|
| Graphit-iC | 13.9 | 181 | 0.077 | 0.082 |
| Dymon-iC | 17.0 | 139 | 0.122 | 0.253 |

H and E data previously reported in [47,48].

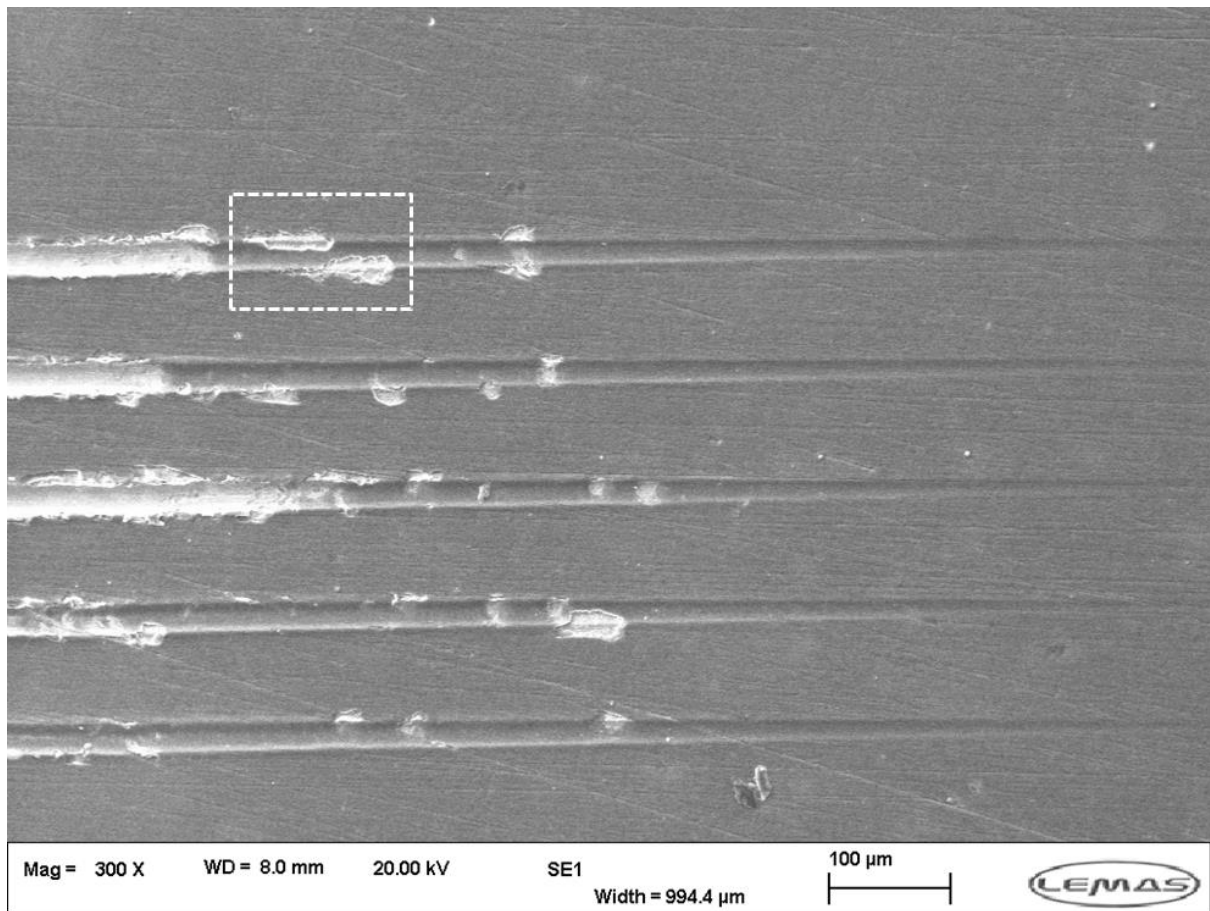
Table 1 (b) Nano-impact data

| | Final depth at 1 mN | Final depth at 5 mN | Final depth at 15 mN |
|------------|-----------------------------|-----------------------------|-----------------------------|
| Graphit-iC | $(0.6 \pm 0.2) \mu\text{m}$ | $(1.5 \pm 0.2) \mu\text{m}$ | $(2.5 \pm 0.2) \mu\text{m}$ |
| Dymon-iC | $(1.0 \pm 0.4) \mu\text{m}$ | $(2.1 \pm 0.2) \mu\text{m}$ | $(3.9 \pm 0.3) \mu\text{m}$ |

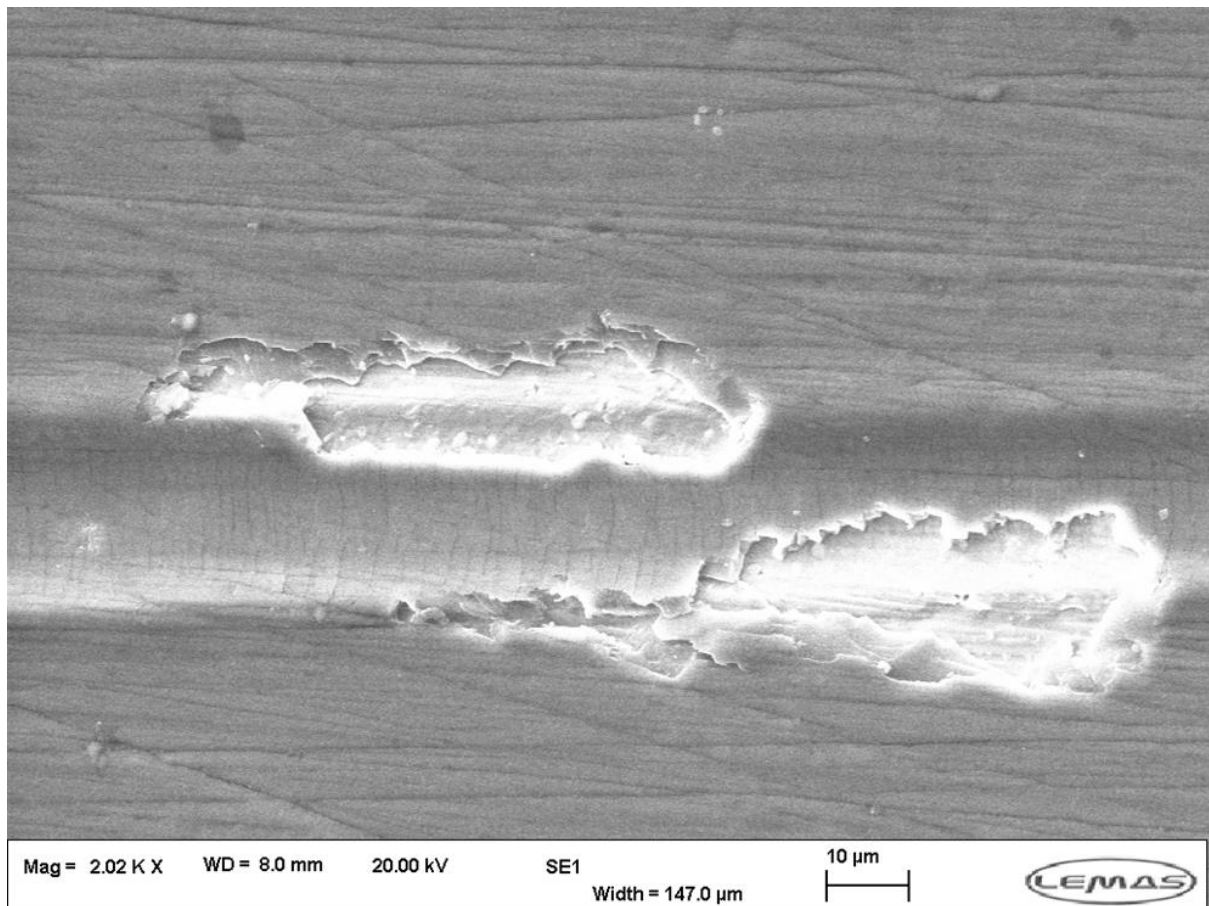
Final impact depth under load after 450 impacts with cube corner diamond probe accelerated from 15 μm above the surface. Data previously reported in [47,48].

Table 2 Critical loads in micro-scratch test

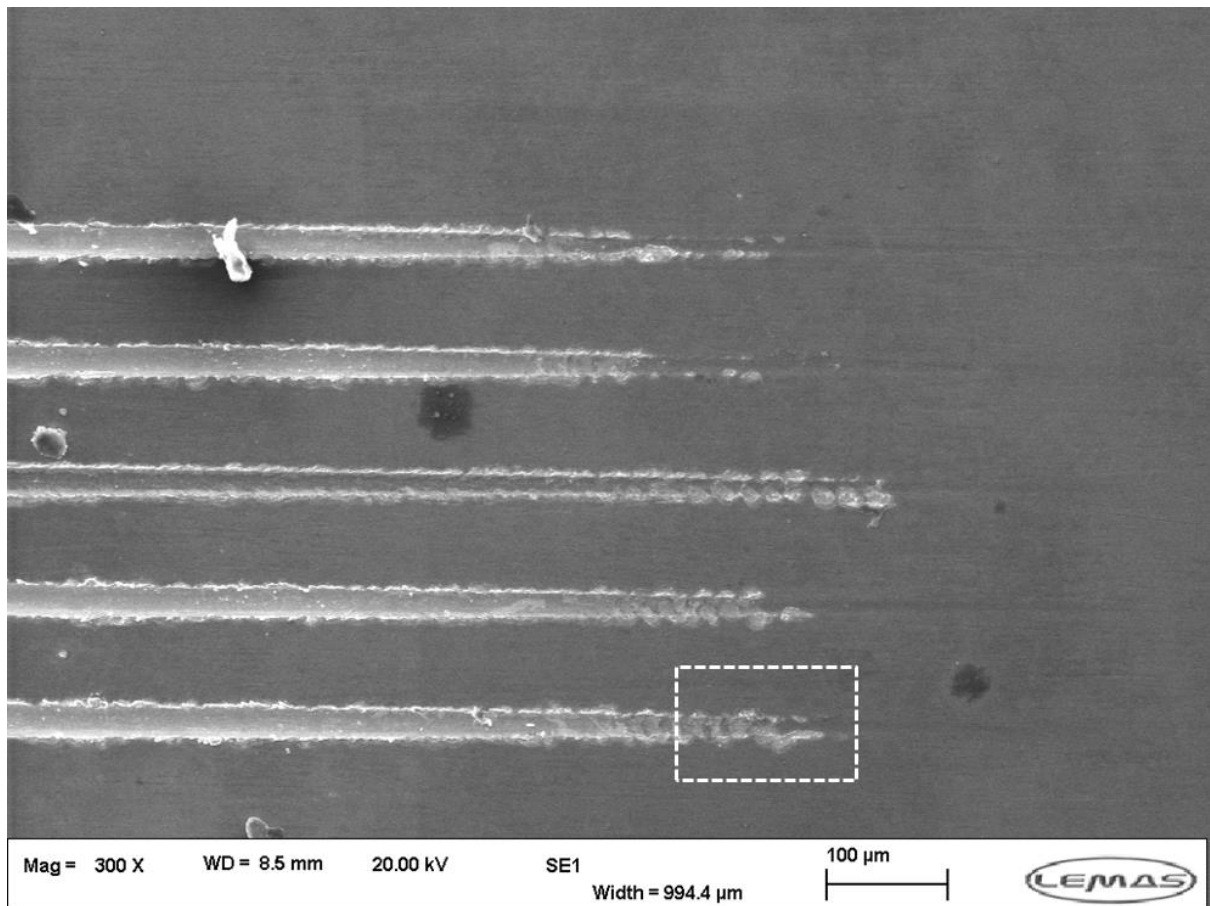
| | Scratching direction relative to machining marks | $L_y (\text{mN})$ | $L_{c1} (\text{mN})$ | $L_{c2} (\text{mN})$ |
|------------|---|-------------------|----------------------|----------------------|
| Graphit-iC | Perpendicular | 200 ± 23 | 2113 ± 86 | 2622 ± 101 |
| Graphit-iC | Parallel | 273 ± 32 | 1990 ± 114 | 2943 ± 255 |
| Dymon-iC | Parallel | 392 ± 280 | 916 ± 242 | 1216 ± 275 |



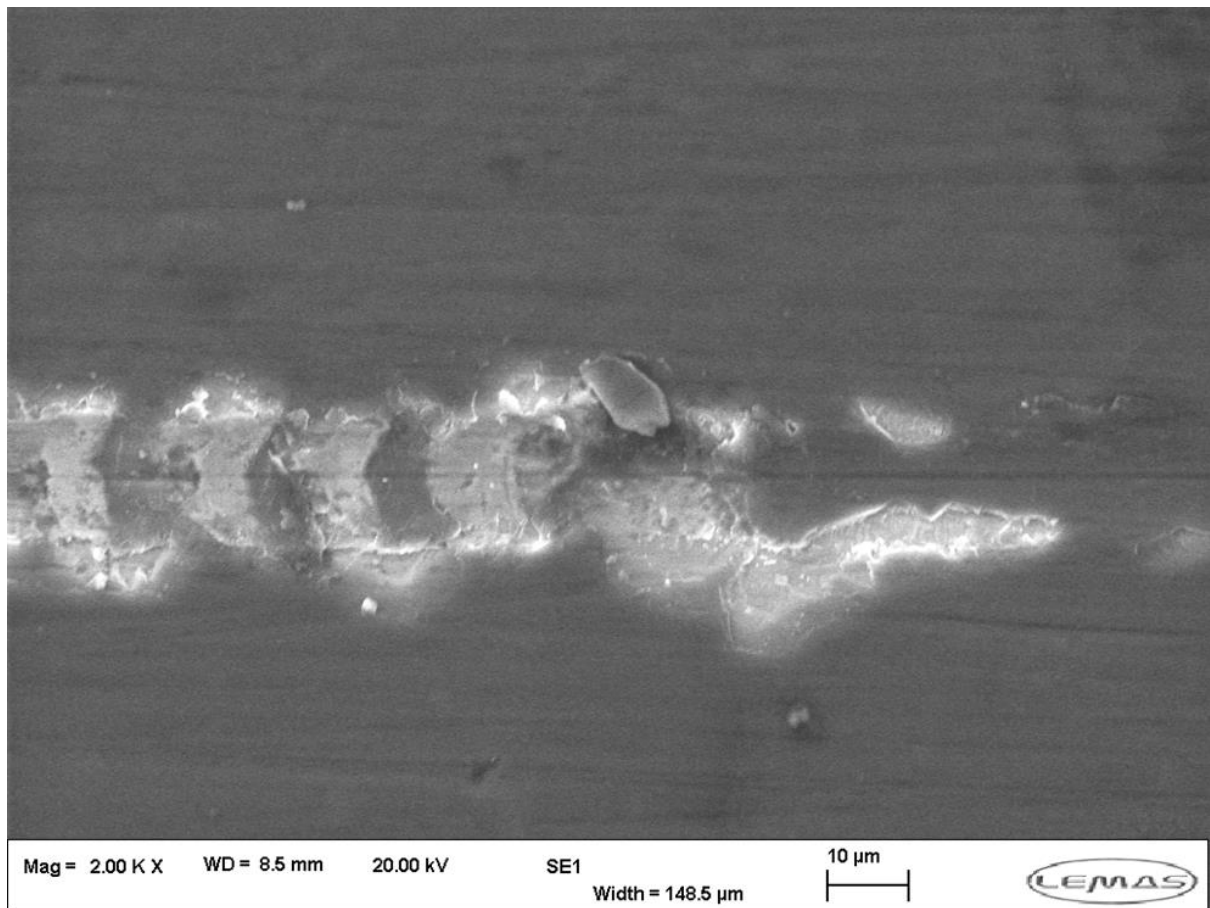
1 (a)



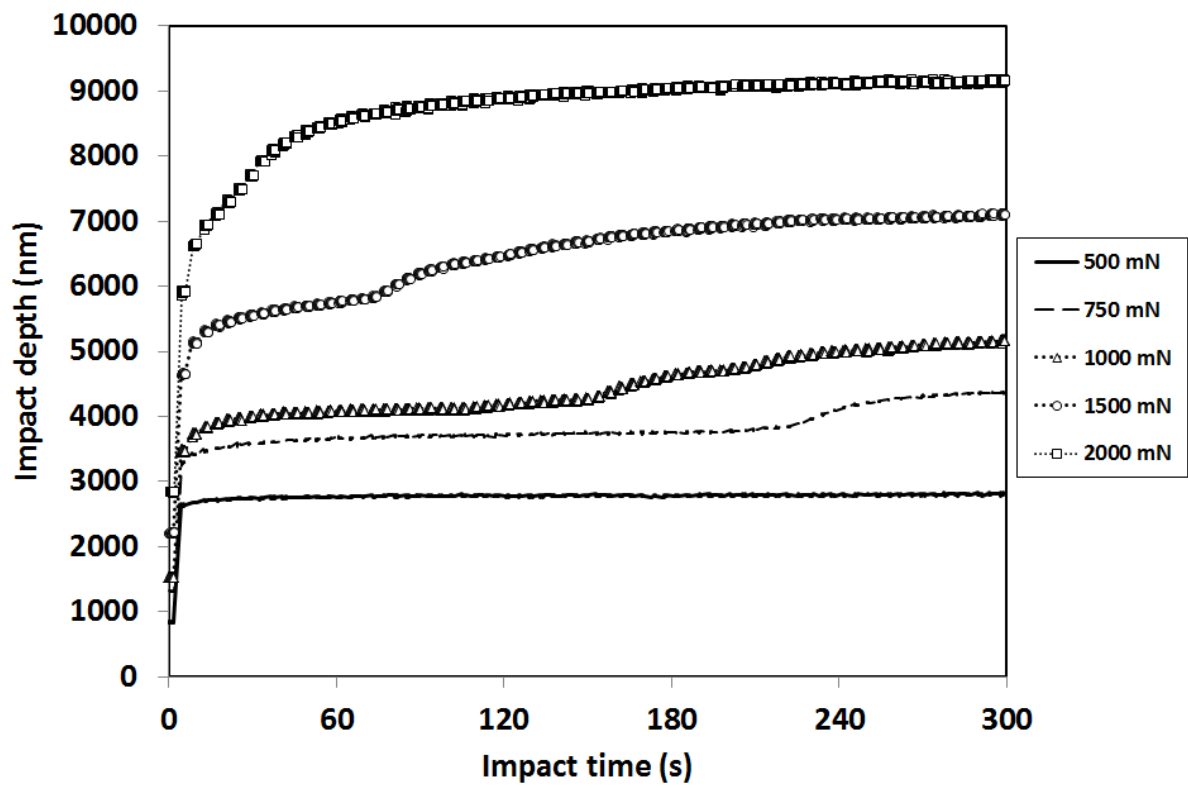
1 (b)



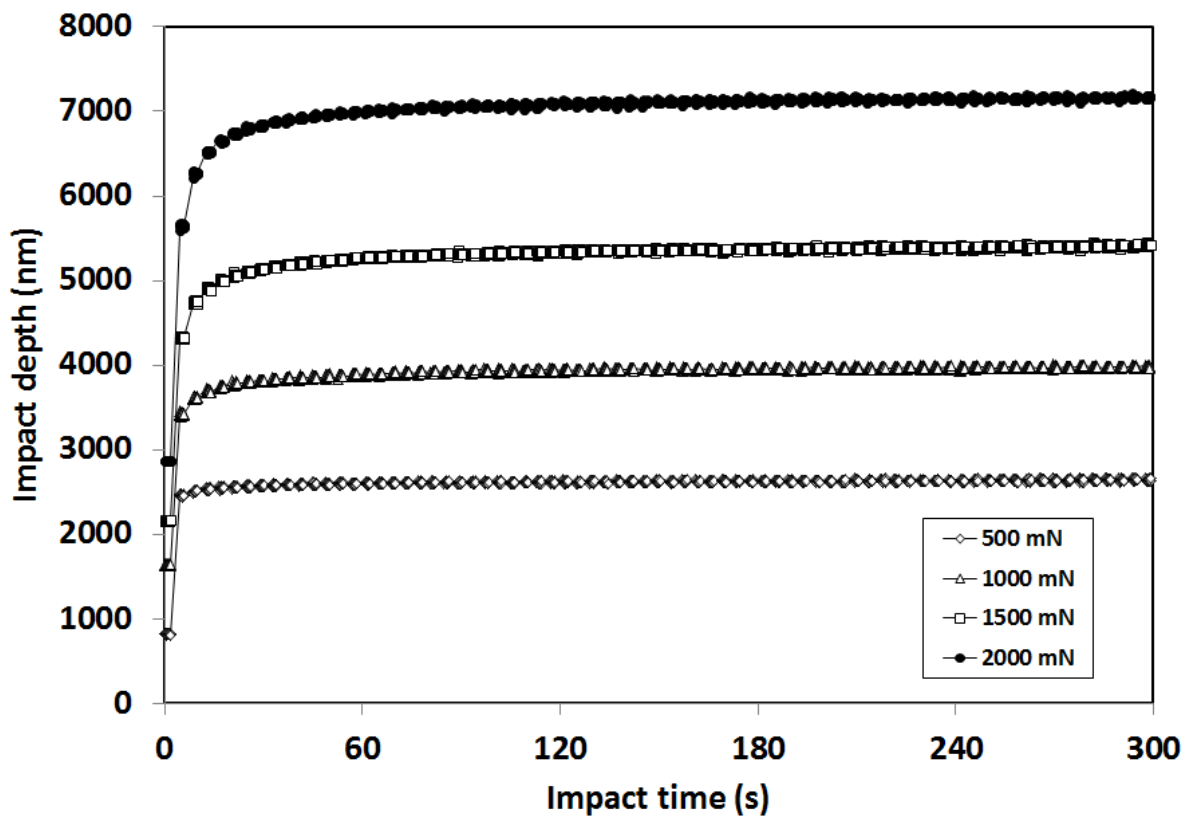
1 (c)



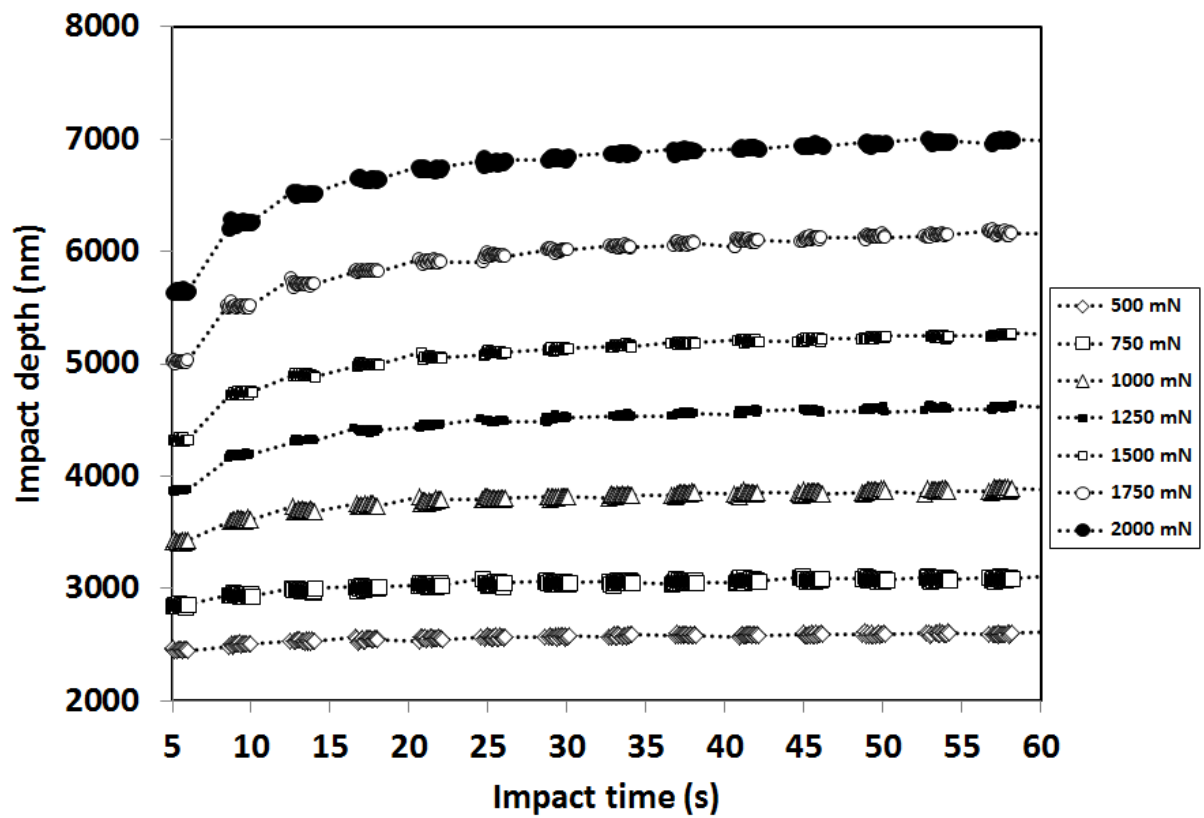
1 (d)



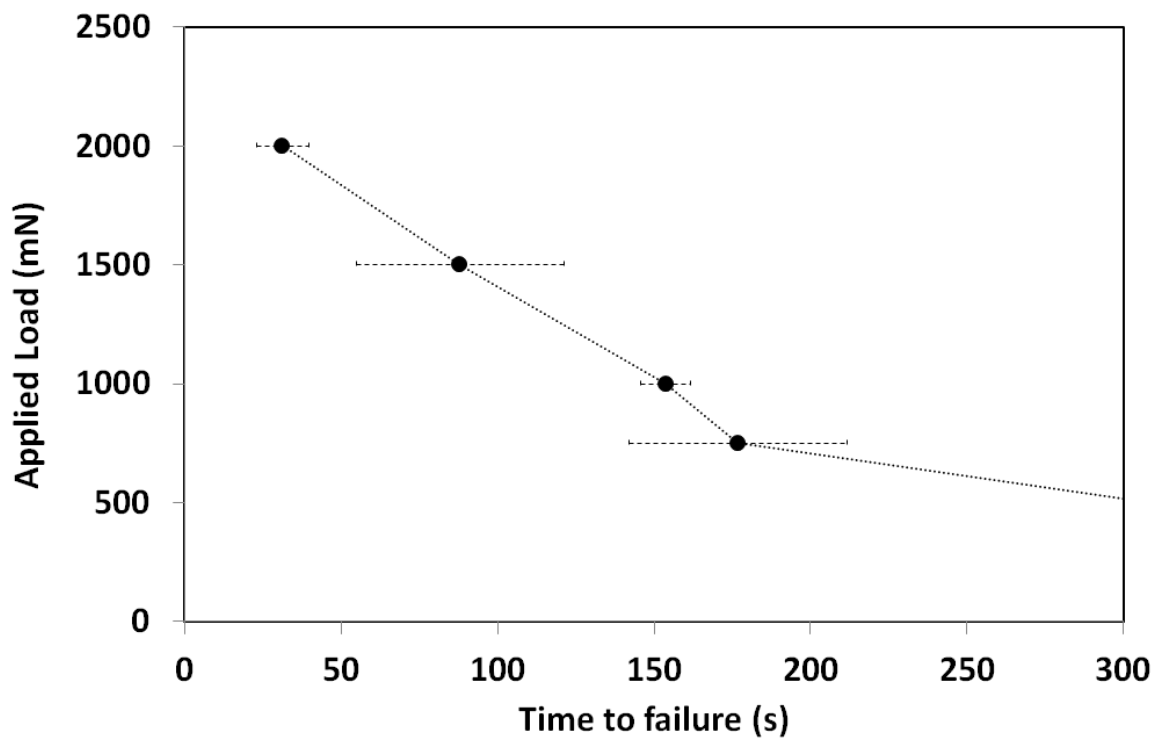
2 (a)



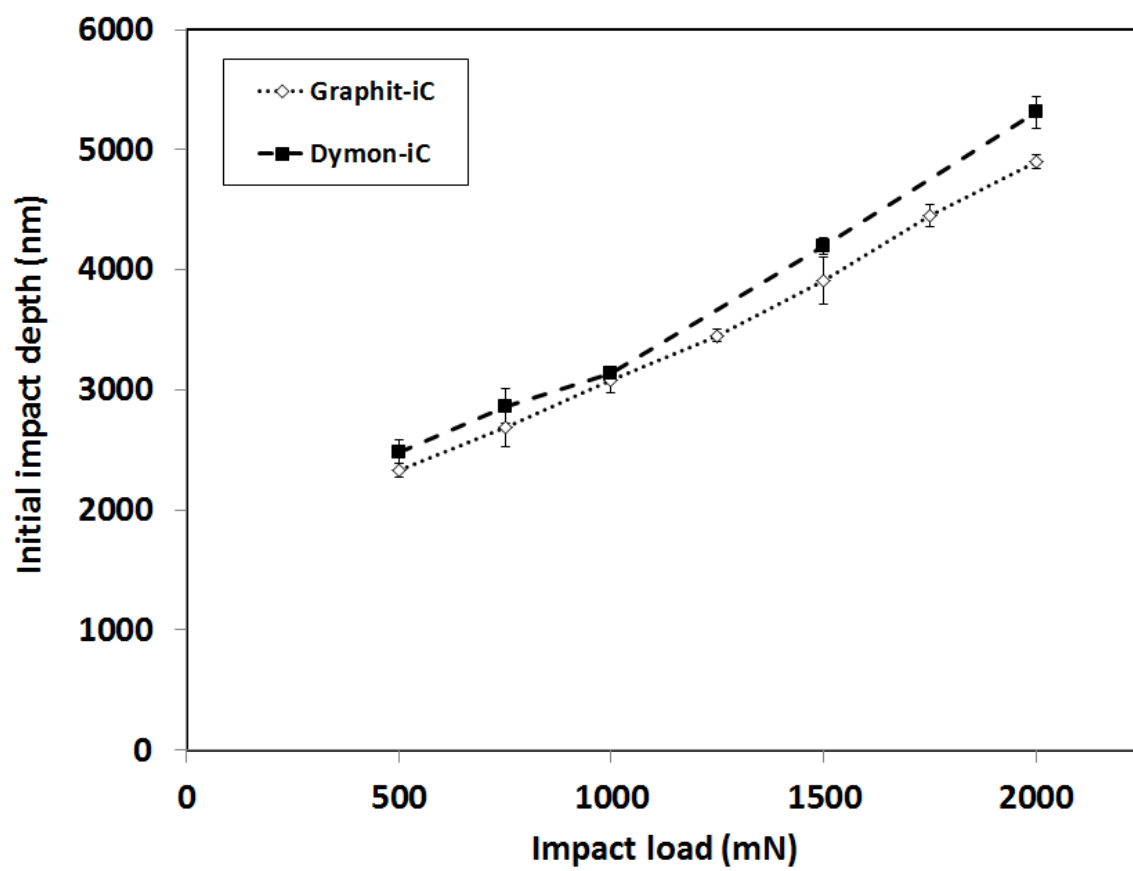
2 (b)



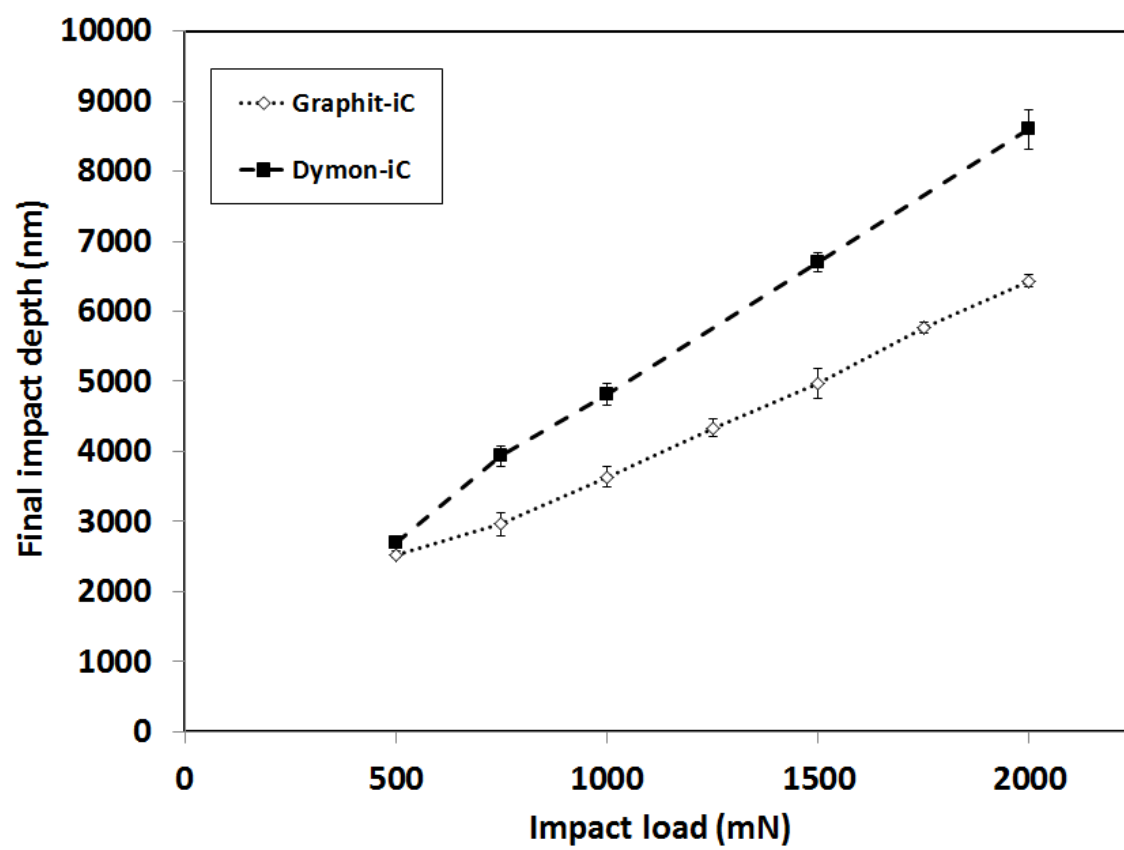
2 (c)



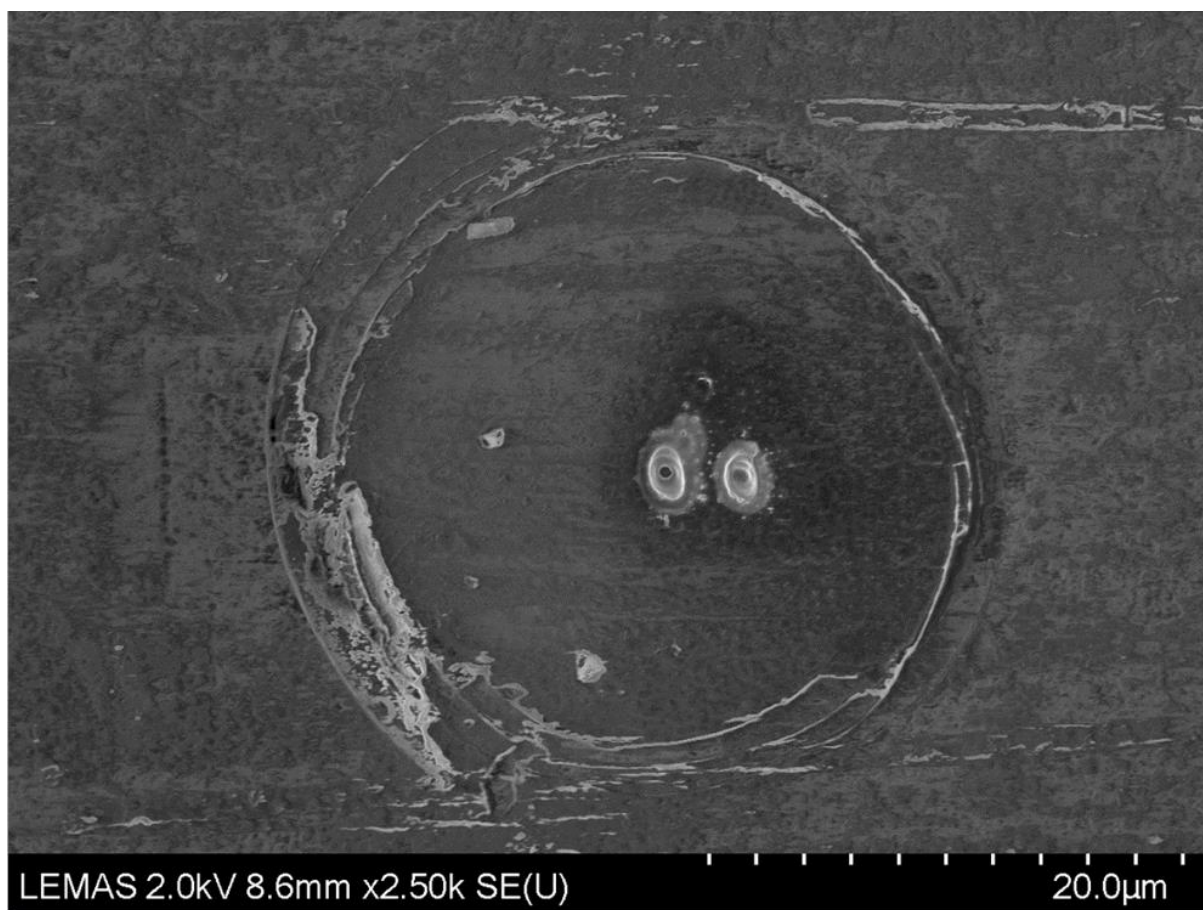
2 (d)



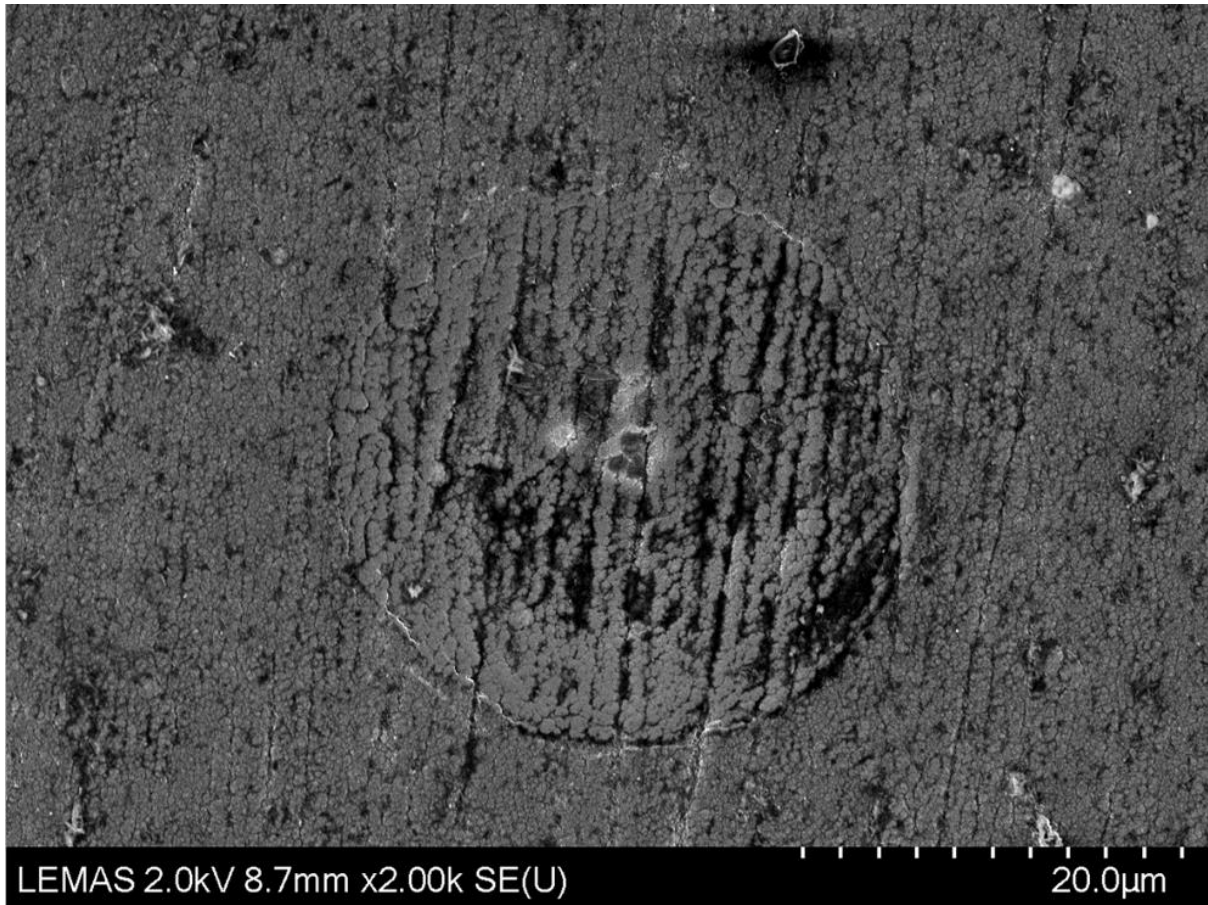
3 (a)



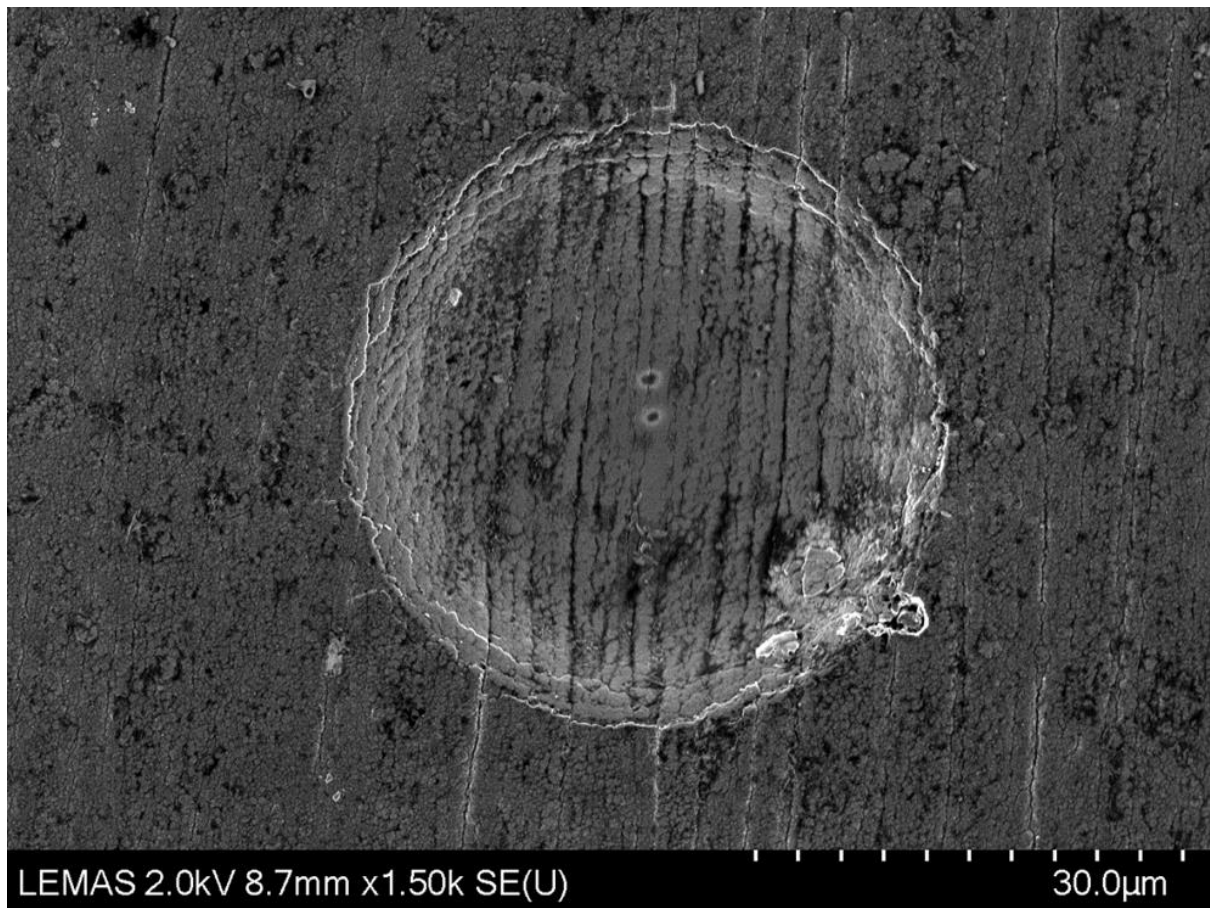
3 (b)



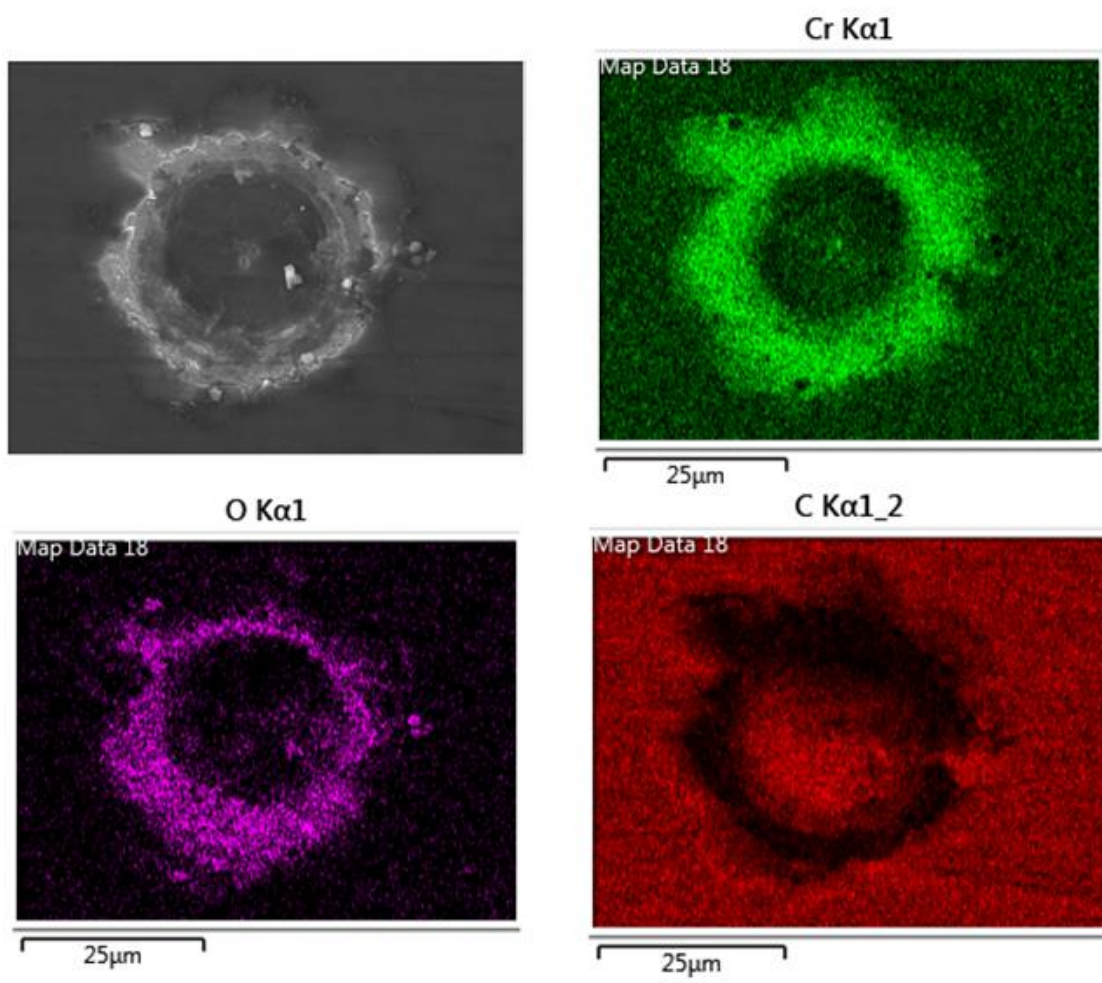
4 (a)



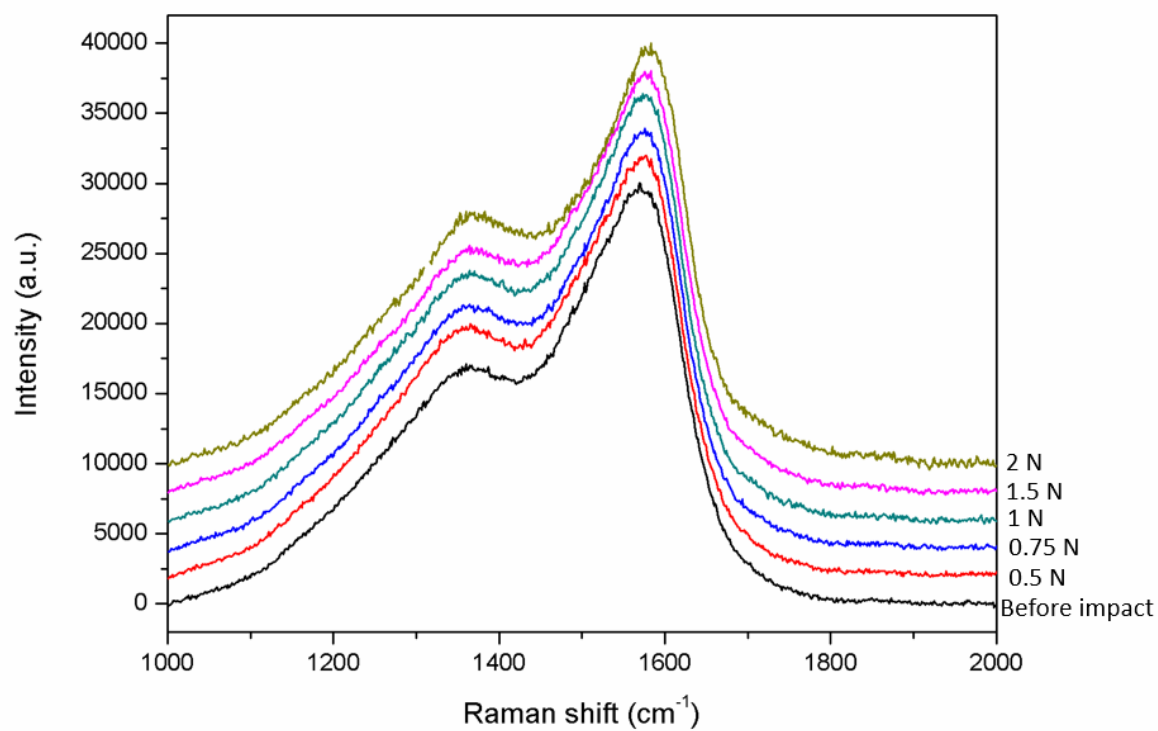
4 (b)



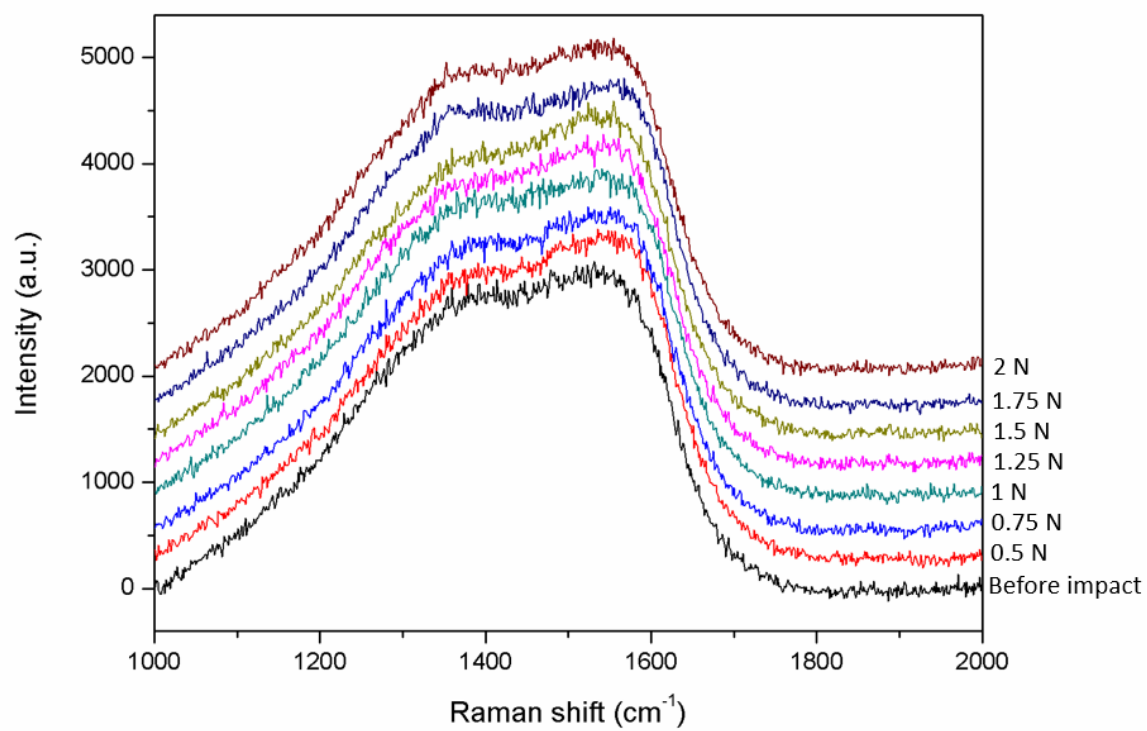
4 (c)



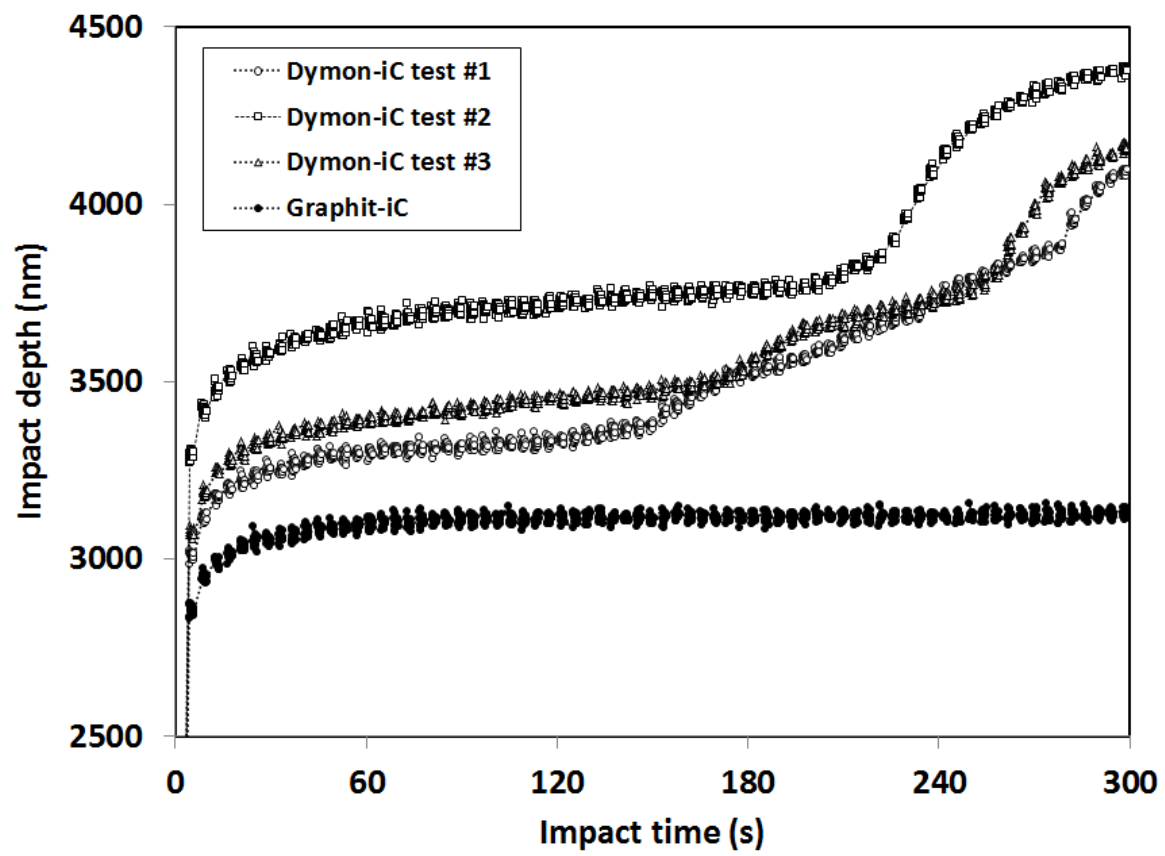
4 (d)



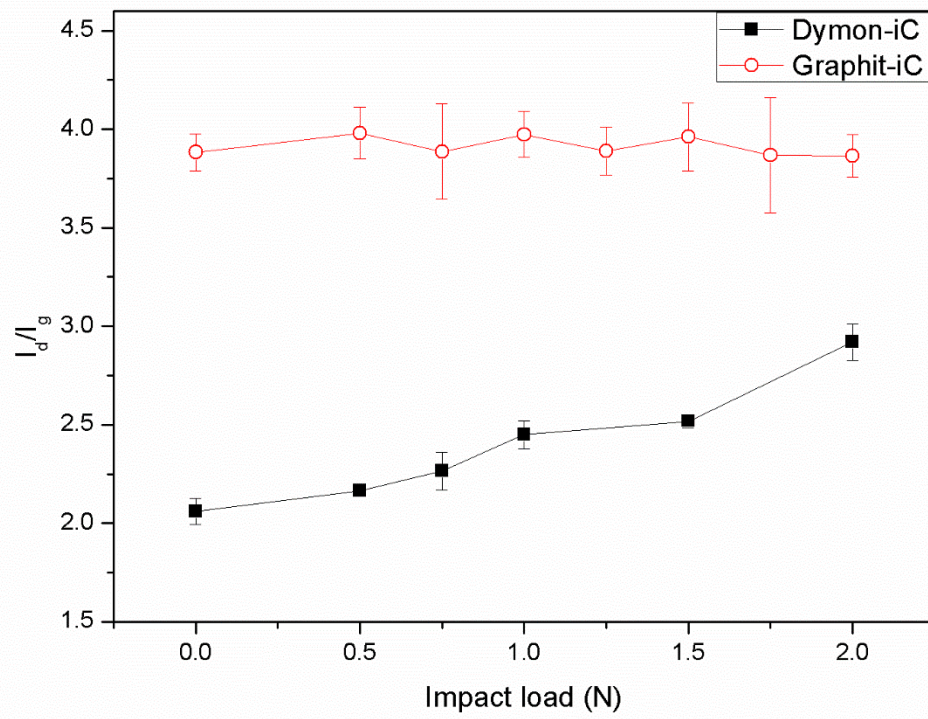
5 (a)



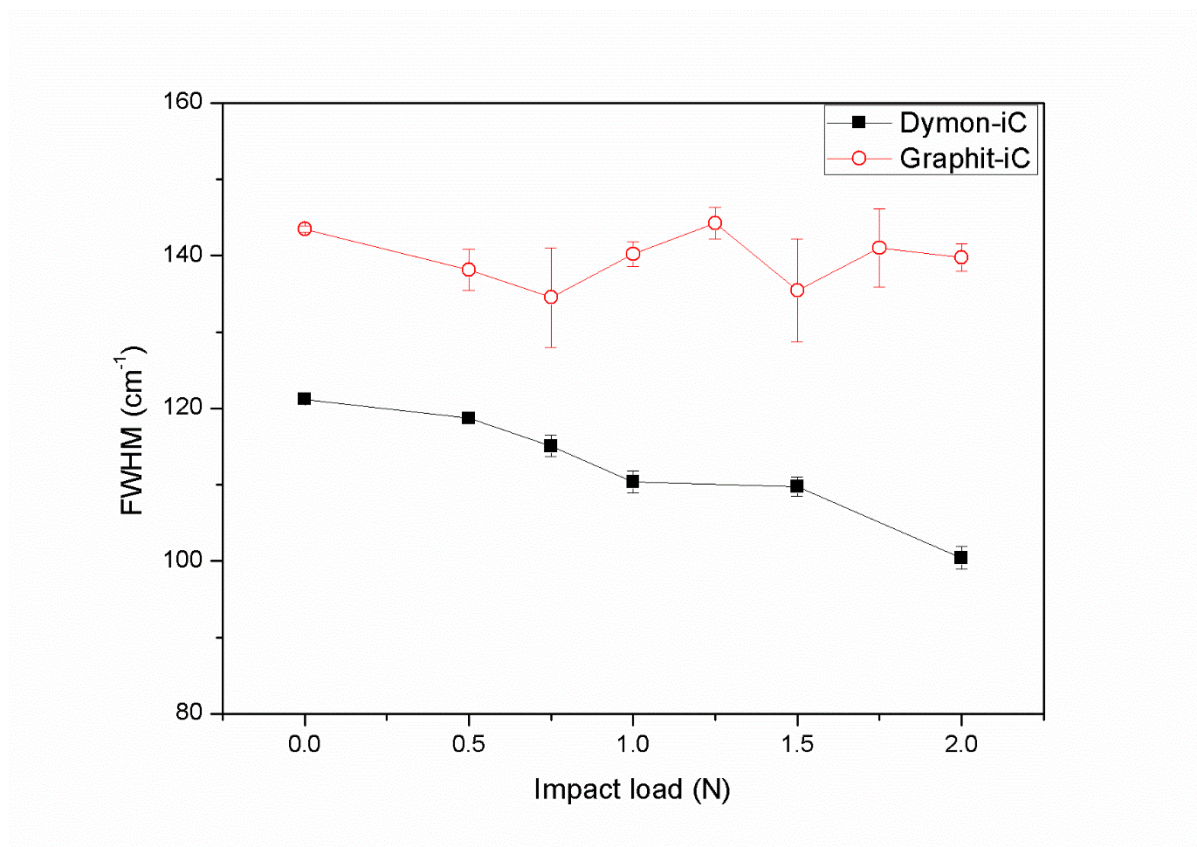
5 (b)



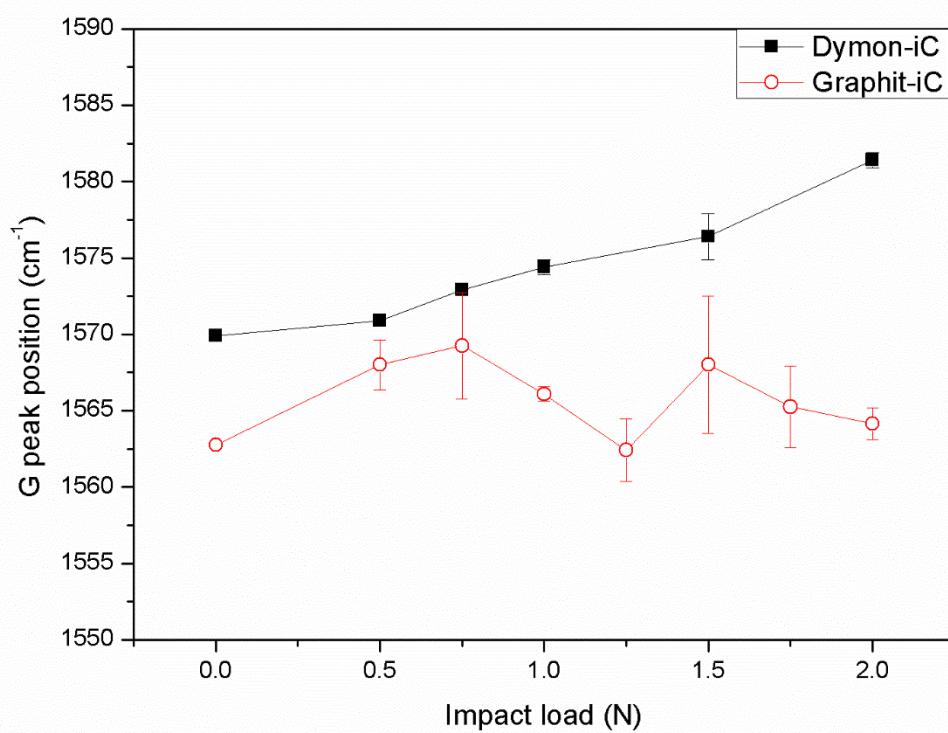
6.



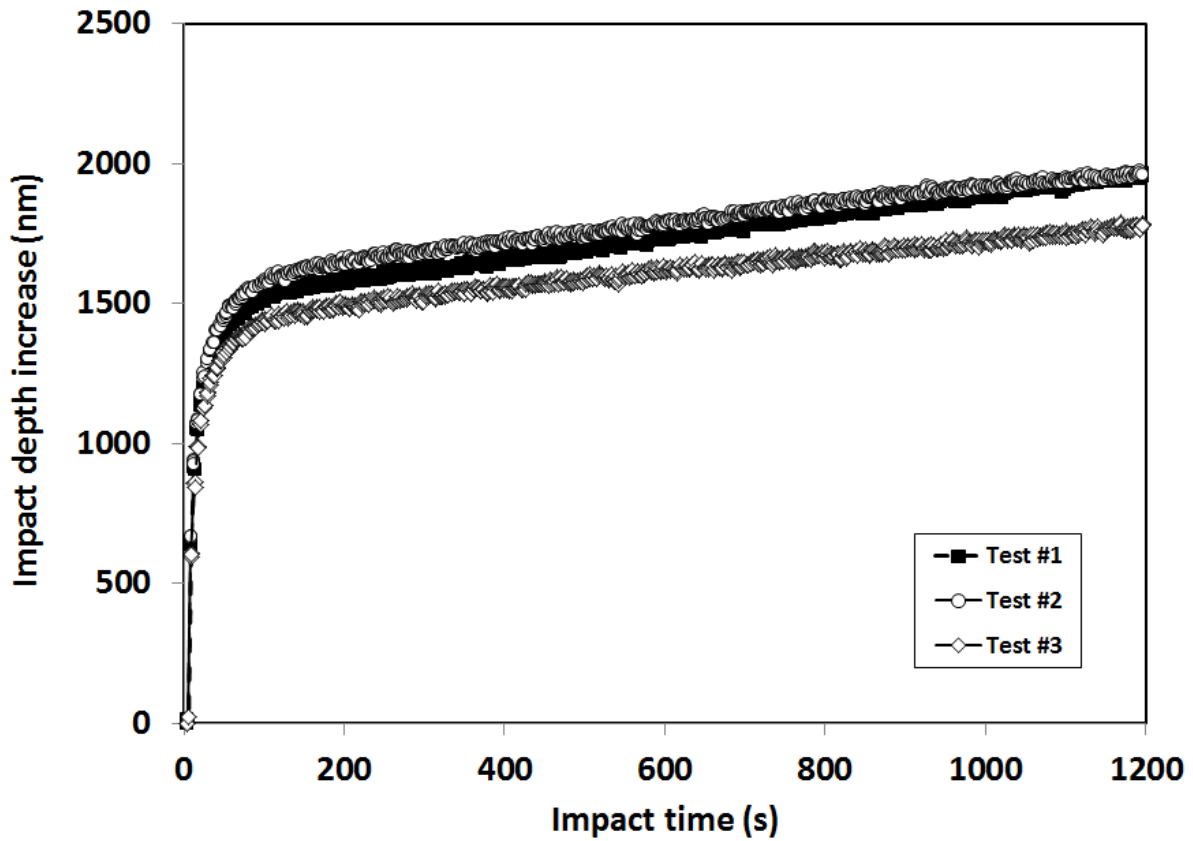
7 (a)



7 (b)



7 (c)



8.

Figure captions

1. SEM images of micro-scratch tracks (a) Graphit-iC, (b) higher magnification image of the boxed region in (a), (c) Dymon-iC, (d) higher magnification image of the boxed region in (c). The scratch direction is right to left.
2. Illustrative impact depth vs. time plots for (a) Dymon-iC (b) Graphit-iC (c) 0-60 s on Graphit-iC. (d) Time to failure on Dymon-iC.
3. (a) Load dependence of (i) initial impact depth (ii) final impact depth.
4. (a) SEM image of (i) Dymon-iC at 0.5 N (ii) Graphit-iC at 0.5 N (iii) Graphit-iC at 1.75 N (iv) Dymon-iC at 1 N with C, Cr, and O EDX maps.
5. Raman spectra of (a) Dymon-iC (b) Graphit-iC.
6. Evolution of probe depth in tests at 0.75 N

7. Load dependence of (a) I_d/I_g (b) FWHM and (c) G-peak position in Raman spectra from the centre of the impact craters
8. Increase in probe depth during 1200 s tests at 2 N on Graphit-iC.